Lithos 394–395 (2021) 106139

Contents lists available at ScienceDirect

Lithos

journal homepage: www.elsevier.com/locate/lithos

Research Article

Garnet perspectives on the metamorphic history and tectonic significance of Paleoproterozoic high-pressure mafic granulites from the northern Hengshan, North China Craton

Jia-Lin Wu [a,b,*], Ming-Guo Zhai [c,d], Bo Hu [a,*], Hua-Feng Zhang [e], Xu Chu [f], Ning-Chao Zhou [g], Le Zhang [h], Hong Zhang [b]

[a] School of Earth Science and Resources, Chang'an University, Xi'an 710054, China
[b] State Key Laboratory of Continental Dynamics, Department of Geology, Northwest University, Xi'an 710069, China
[c] Key Laboratory of Computational Geodynamics, University of Chinese Academy of Sciences, Beijing 100049, China
[d] Institute of Geology and Geophysics, Chinese Academy of Sciences, Beijing 100029, China
[e] School of Earth Sciences and Resources, China University of Geosciences, Beijing 100083, China
[f] Department of Earth Sciences, University of Toronto, Toronto, ON M5S 3B1, Canada
[g] MLR Key Laboratory for the Study of Focused Magmatism and Giant Ore Deposits, Xi'an Center of Geological Survey, China
[h] State Key Laboratory of Isotope Geochemistry, Guangzhou Institute of Geochemistry, Chinese Academy of Sciences, Guangzhou 510640, China

ARTICLE INFO

Article history:
Received 16 July 2020
Received in revised form 23 March 2021
Accepted 25 March 2021
Available online 29 March 2021

Keywords:
Garnet zoning
Prograde metamorphism
Paleoproterozoic high-pressure mafic granulites
Northern Hengshan
North China Craton (NCC)

ABSTRACT

Reconstructing the pressure-temperature (*P-T*) evolution of early Precambrian high-pressure granulites and eclogites is critical for decoding the tectono-metamorphic evolution of the early Earth. However, debates continue regarding the *P-T* history of these rocks because of various modifications by peak and retrograde rehydration metamorphism. As a significant rock-forming mineral in high-grade metamorphic rocks, garnet not only grows with increasing pressure or temperature and develops variably zoned patterns along given *P-T* loops, but its properties are stable subsequent to its formation when compared to other minerals in the matrix. Consequently, garnet is excellent for monitoring the thermo-metamorphic history of its host rock during orogeny. Selected garnet grains from the Paleoproterozoic high-pressure mafic granulites in the northern Hengshan area of the North China Craton, which exhibit variable microstructural and chemical zoning, present an excellent example for extracting metamorphic evolution of the host rocks. Microstructural zoning displays a zonal distribution of frozen inclusion-type minerals in garnet. Chemically, the garnet shows pronounced compositional zoning, with bell-shaped X_{Sps}, initially flat and then increasing/decreasing X_{Pyr} and Fe#, initially increasing and then decreasing X_{Grs} from core to mantle, and resorbed rims. Both zoning patterns document multiple generations of radial growth history. The progressive evolution of the host rocks can be further divided into early prograde (M_{1-1}), late prograde (M_{1-2}), near peak (M_{2-1}), and peak (M_{2-2}) stages. The resorption textures indicate the succeeding decompression (M_3) and cooling (M_4) stages. The pseudosection modeling indicates *P-T* conditions from M_{1-1} to M_{2-1} of 6–9 kbar/600–700 °C, 9–11.2 kbar/680–740 °C and 12–15 kbar/735–785 °C, respectively. Although the peak metamorphic information of M_{2-2} is lost because of the breakdown of the garnet rim, plausible *P–T* results are estimated at ~15–17 kbar/~790–810 °C. These conditions prevailed to the transitional eclogite-granulite facies through qualitative reconstruction of the original composition of clinopyroxene, modal proportion, and rim composition of the garnet. The subsequent conditions of decompression (M_3) and cooling (M_4) stages were roughly estimated at ~7–10 kbar/~800–850 °C and 3–5 kbar/ 650–680 °C. Together, they define a clockwise *P-T* path in response to the Paleoproterozoic orogeny involved in the assembly of the North China Craton. The zoned garnet suggests that the host mafic granulite documents a relatively complete progressive metamorphic history, which probably correlates with subduction processes. The resorbed rim sequentially records exhumation and cooling processes. Furthermore, the preservation of growth zoning in granulitic garnet and near-isothermal decompression *P-T* path suggests that the host rocks must have experienced a very short peak metamorphism and a rapid exhumation process to the middle crust. These findings suggest that the tectonic processes involved in the formation of the Paleoproterozoic northern Hengshan granulite terrane might be similar to those of the Phanerozoic continental collisional orogens under modern plate tectonic regimes; however, they record relatively higher apparent thermal gradients (~14–16 °C /km).

* Corresponding authors at: School of Earth Science and Resources, Chang'an University, Xi'an 710054, China.
E-mail addresses: wjl_nwu@163.com (J.-L. Wu), hubowork@126.com (B. Hu).

https://doi.org/10.1016/j.lithos.2021.106139
0024-4937/

1. Introduction

High-pressure granulites and moderate-temperature eclogites of the Paleoproterozoic age have been identified on many continents, recently. Examples includes: the Snowbird tectonic zone (Baldwin et al., 2007) and the Trans-Hudson orogen (Weller and StOnge, 2017) of Canada, the Belomorian mobile belt of Russia (Liu et al., 2017), the Eburnian-Transamanzonian orogen (Loose and Schenk, 2018) and the Ubendian-Usagaran belt (Brown et al., 2020) of Africa, the Nagssugtoqidian orogen of Greenland (Müller et al., 2018), and the Trans-North China Craton Orogen of China (Guo et al., 2002; Wan et al., 2015; Wu et al., 2016; Xu et al., 2018; Zhai et al., 1992, 1995; Zhang et al., 2018, 2020a; Zhao et al., 2001). These rocks display contrasting thermo-metamorphic records with those of the Archean, when low- to moderate-pressure metamorphosed terranes were dominant (e.g., Windley, 1995; Brown, 2007; Brown and Johnson, 2018; Holder et al., 2019; Palin et al., 2020). Consequently, studies regarding the *P-T* evolution of the widespread Paleoproterozoic high-pressure granulites and eclogites are believed to provide critical information to understand the thermomechanics of early plate tectonics (e.g., Zhai, 2009, 2012; Sizova et al., 2010; Perchuk and Morgunova, 2014; Zhou et al., 2017; Holder et al., 2019; Brown and Johnson, 2018; Palin et al., 2020).

However, debates continues regarding the pressure-temperature (*P-T*) history of the early Proterozoic high-pressure granulites and eclogites found globally. *P-T* histories derived from most of these rocks involve near-isothermal decompression, uncertain prograde records, and peak conditions (e.g., Baldwin et al., 2007; Liu et al., 2017; Loose and Schenk, 2018; Zhai, 2009; Zhao et al., 2001). The metamorphic evolution of Paleoproterozoic high-pressure mafic granulite terranes from northern Hengshan in the North China Craton (NCC) presents such an example (e.g., Zhai, 2009; Zhai et al., 1995; Zhang et al., 2018; Zhao et al., 2001). Considerable attention has been paid to the metamorphic evolution of the high-pressure granulites in the northern Hengshan area since their discovery in the 1990s (Wang et al., 1991; Zhai et al., 1995); however, many issues remain unresolved. The inferred protoliths of these mafic granulites mainly occur as mafic dykes or sills intruding into country rocks consisting predominantly of granitic orthogneisses (Kröner et al., 2006; Li et al., 1998; O'Brien et al., 2005). Several major concerns regard if these mafic lithologies were metamorphosed in situ at the base of the continental crust or experienced common burial histories with their surrounding rocks from upper to deep crustal levels and the exact *P-T* conditions of peak metamorphism (e.g., Kröner et al., 2006; O'Brien et al., 2005; Qian et al., 2019; Qian and Wei, 2016; Trap et al., 2011; Wei, 2018; Wei et al., 2014; Zhai, 2009; Zhang et al., 2018; Zhao et al., 2001; Zhou et al., 2017). These debates arise due to the lack of robust multi-generation mineral assemblages in the present-day exposed samples, which might be related to strong modifications during peak and retrograde rehydration metamorphism and/or secondary tectonic overprints (e.g., Maruyama et al., 2010; Zhai, 2009). Moreover, the timing and the interval of granulite-facies metamorphism is still unconstrained due to the lack of correlation between the metamorphic ages and the mineral assemblages (e.g., Zhai, 2009). These uncertainties do not permit robust interpretations of the tectonic evolution of the rocks.

As a significant rock-forming mineral in high-grade metamorphic rocks, garnet not only stablizes over a large *P-T* range and has variable chemical compositions, but it also has robust physical and chemical properties; Consquently, it is resistant to retrograde and rehydration modifications (e.g., Caddick and Kohn, 2013; Spear, 1993). As a result, garnet is a better monitor of the tectono-metamorphic evolution of its host rocks than other minerals in the matrix (e.g., Maruyama et al., 2010; Parkinson, 2000). A recent study regarding garnet compositional zoning of high-pressure mafic granulites from the northern Hengshan area documented evidence of late prograde metamorphism prior the peak stage (Zhang et al., 2018). It is important for understanding the metamorphic history of the high-pressure granulites, although no prograde mineral assemblages were presented and unsuitable activity-composition (A-X) relationships for metapelitic component systems (White et al., 2007) were used in their pseudosection calculations. In this study, new perspectives from microstructural and chemical zoned garnet are taken to attempt a reconstruction of multi-stage relict mineral assemblages and *P-T* history of the northern Hengshan high-pressure mafic granulites with the newly developed A-X relationships for high-temperature metabastic component systems by Green et al. (2016). The results differ from those of previous studies: (1) zoned granulitic garnet in the studied sample records robust inclusion-type pre-peak mineral assemblages and chemical zoning evidence for progressive metamorphism from early to late stages; (2) well-preserved major element zoning of granulitic garnet and near-isothermal decompression *P-T* path suggest short-period peak metamorphism and rapid exhumation and cooling history from lower to middle crustal levels. These findings provide new clues into the metamorphism and tectonic significance of the Paleoproterozoic high-pressure mafic granulites from the study area.

2. Geological background

During the Paleoproterozoic, the NCC was involved in a series of rifting-accretion-collision processes and developed three mobile belts, which assembled the NCC as a uniform block. The three mobile belts include the Fengzhen mobile belt (Khondalite belt), the Jinyu mobile belt (Trans-North China orogen, TNCO), and the Liaoji mobile belt (Jiao-Liao-Ji belt) (Fig. 1; Zhai and Liu, 2003; Zhao et al., 2005).

The Hengshan Complex is in the north-central part of the Jinyu mobile belt and is exposed as a N*E*-SW-trending mountain, separated from the Huai'an Complex to the north by the Sanggan River and from the Wutai Complex to the south by the Hutuo River (Figs. 1 and 2). This complex is further divided into two parts: the northern Hengshan and southern Hengshan lithotectonic units by the Zhujiafang shear zone in the center of the Hengshan Complex. The rocks mainly consist of Archean tonalitic, trondhjemitic, and granodioritic (TTG) gneisses and granitic gneisses, and some enclaves of mafic fragments and supracrustal rocks, with a decreasing metamorphic grade traveling from north to south (O'Brien et al., 2005; Qian and Wei, 2016; Wei, 2018; Wei et al., 2014). The northern Hengshan mainly consists of granulite-facies TTG and granitic gneisses, migmatites and garnet mafic granulite boudins or lenses, although some original mineral assemblages were retrogressed to amphibolite facies. The southern Hengshan mainly consists of amphibolite-facies TTG and granitic gneisses and metasupracrustal rocks, with some metamafic lenses. The Zhujiafang shear zone trends E-W and comprises mylonitic feldspathic gneisses, amphibolites, mica schists, banded iron formations, and quartzite (Li and Qian, 1994; Zhang et al., 2007; Trap et al., 2011).

Zircon U–Pb ages revealed that the TTG and granitic gneisses dominantly intruded at 2.52–2.48 Ga (Kröner et al., 2005), and minor granitic gneisses formed at 2.35–2.05 Ga (Kröner et al., 2005; Zhao et al., 2011). Sequentially, these rocks were commonly metamorphosed at ~1.95–1.85 Ga. These were further divided into two metamorphic clusters at ~1.95 Ga and ~ 1.85 Ga, and were interpreted as metamorphic ages of peak and retrograde metamorphism, respectively (e.g., Qian and Wei, 2016; Zhang et al. 2016a, 2018). They suggest that the northern Hengshan terrane has suffered prolonged (~100 Ma) metamorphism. Recently, Qian et al. (2019) proposed a new interpretation that the latter ~1.85 Ga might represent another episode of intraplate collisional events (Wei, 2018). Coeval with these high-grade metamorphic events,

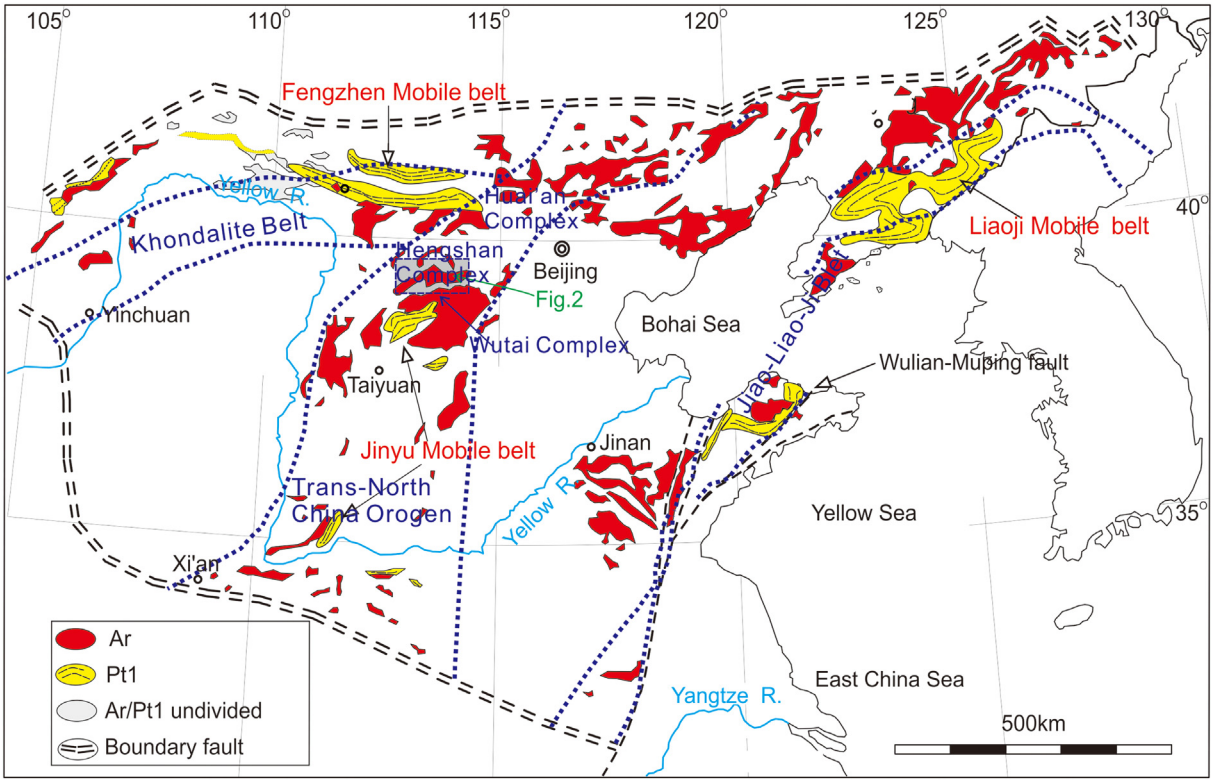

Fig. 1. Paleoproterozoic mobile belts and distribution of early Precambrian rocks in the North China Craton (Zhai and Liu, 2003). Dashed blue lines represent the boundary of three different continental collisonal orogenic belts proposed by Zhao et al. (2005). Ar-Archean, Pt1-Paleoproterozoic. (For interpretation of the references to colour in this figure legend, the reader is referred to the web version of this article.)

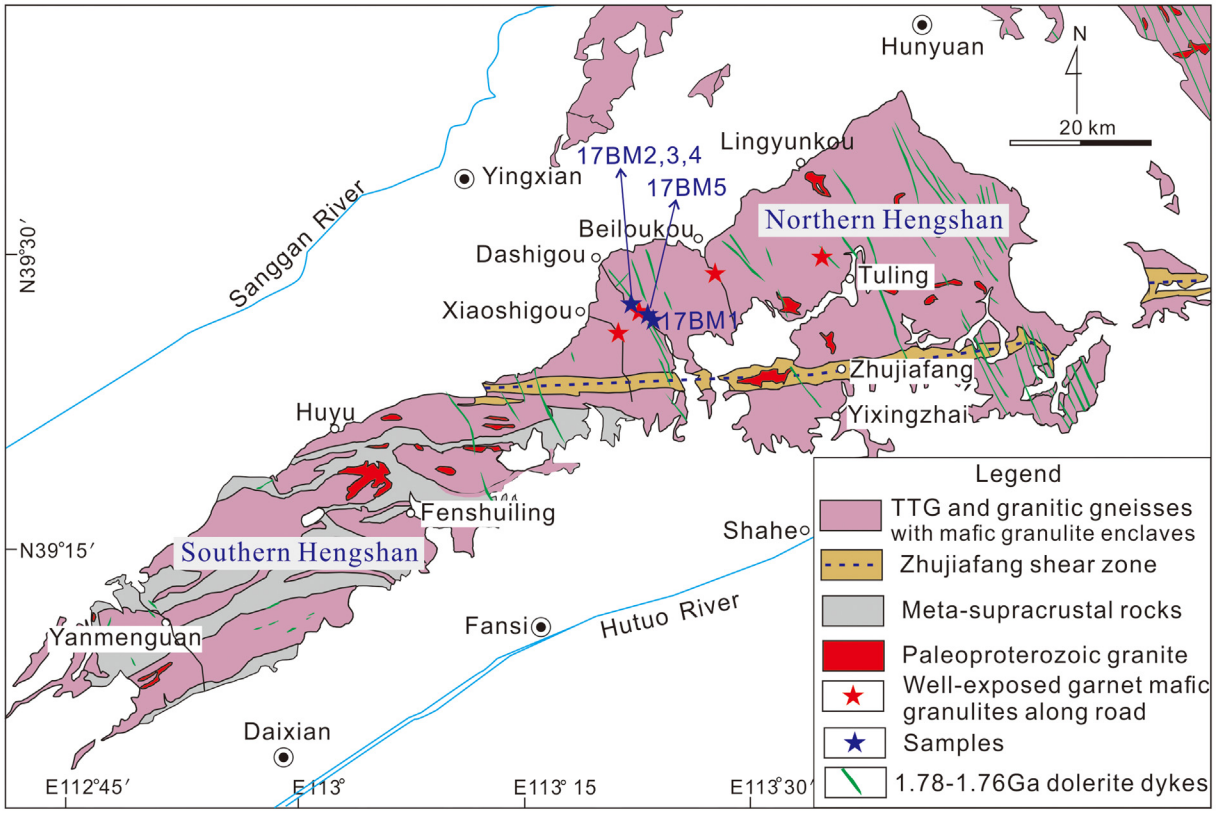

Fig. 2. Geological sketch map of the Hengshan Complex (modified after Zhao et al., 2011).

a minor anatectic granite appeared (Kröner et al., 2006). The amphibole and mica $^{40}Ar/^{39}Ar$ ages and metamorphic zircon ages suggest that the shear deformation event occurred at 1.86–1.80 Ga (Qian et al., 2019; Trap et al., 2012). Rutiles in the high-pressure granulites from northern Hengshan and adjacent Huai'an area document U–Pb ages of ~1.75 Ga, which were interpreted as resetting ages by extensive and intensive 1.78–1.76 Ga dolerite dyke swarms events in the northern part of the central NCC (e.g., Halls et al., 2000; Peng et al., 2005; Zhang et al., 2020b).

The high-pressure mafic granulites mainly occur as boudins and lenses included in the TTG gneisses of the northern Hengshan area (Fig. 3a; Wang et al., 1991; Zhai et al., 1995; Li et al., 1998; Kröner et al., 2006; Wei, 2018). Granitic melt patches occur in these mafic boudins, which might result from in-situ partial melting during near-isotheraml decompression process (Kröner et al., 2006; Trap et al., 2011). More detailed field occurrences of these high-pressure mafic granulites are presented in Kröner et al. (2006). The mafic granulites were metamorphosed at transitional eclogite-granulite facies conditions and are considered counterparts of high-pressure metamorphic terranes in the phanerozoic collisonal orogens (e.g.,Zhai et al., 1995 ; Zhao et al., 2001). Hence, they are believed to be significant petrological evidence for inferring the assembly processes of the NCC (Zhai et al., 1995; Zhao et al., 2001). Their protoliths were considered mafic dykes intruding into their surrounding TTG and granitic gneisses, which suggested an early extensional event prior high-grade metamorphism (Kröner et al., 2005, 2006; Li et al., 1998; Wei et al., 2014). The mineralogy consists of garnet-clinopyroxene-bearing assemblages, with some quartz, rutile, plagioclase, ilmenite, and amphibole. Previous studies suggest that the high-pressure mafic granulites record three metamorphic stages (M_1-M_3): M_1 represents the peak-pressure stage with metamorphic conditions of high-pressure granulite to eclogite facies; M_2 represents medium-pressure granulite-facies decompression; and M_3 features amphibolite-facies metamorphism (O'Brien et al., 2005; Zhai et al., 1995; Zhao et al., 2001). No robust prograde metamorphic information has been observed in the granulites, comparable to those from the metamorphic features of garnet mafic granulites from the Huai'an–Chengde area of the north-central NCC (Zhai, 2009 and references therein). Recently, a few new lines of evidence from composition zoning in garnet suggest that high-pressure mafic granulites from the northern Hengshan area (Zhang et al., 2018), as well as those from the Huai'an-Chicheng area (Guo et al., 2002; Wu et al., 2018a; Zhang et al. 2016b, 2020a), probably have documented a period of prograde metamorphism before the peak metamorphic stage. However, there is no robust petrographic evidence of progressive metamorphism has been present. This may be because the microstructural zoning of garnet in granulite did not receive due attention. Here, textural zonation and compositional zoning of garnet in mafic granulite from the northern Hengshan area were investigated in detail.

3. Analytical methods

Mineral compositions were analyzed with a JEOL JXA-8230 electron microprobe under conditions of a 15-kV accelerating voltage and 10-nA probe current with a 1-μm diameter beam. Data were regressed using the ZAF correction method. The experiments were conducted at the State Key Laboratory of Continental Dynamics, Northwest University, China, and the MNR Key Laboratory for the Study of Focused Magmatism and Giant Ore Deposits, Xi'an Center of Geological Survey, China. Sample 17BM5 was selected for detailed mineral composition analysis, and the representative mineral compositions are listed in Table 1. The ferric iron content of minerals was estimated by the charge balance method of Droop (1987). The bulk rock composition of sample 17BM5 was measured on fused glass beads using X-ray fluorescence spectrophotometry at Nanjing Hongchuang Geological Exploration Technology Service Co., Ltd., Nanjing, China.

4. Petrology and mineral chemistry

Five representative samples (17BM1to −5) were collected from the Dashigou Valley (Fig. 2). They are coarse-grained garnet mafic granulites with mineral assemblages of garnet (15%–45%), clinopyroxene (20%–35%), plagioclase (5%–10%), amphibole (5%–10%), quartz (5%–10%), rare orthopyroxene (1%–3%), biotite (<2%), rutile, titanite, ilmenite, apatite, and sulfides (Fig. 3b-f).

After scanning through the whole thin section under a microscope, representative garnet grains of the largest ones with obvious microstructural zoning were selected for compositional profile analysis and X-ray mapping, because this type of garnet is expected to potentially cut through the center of the crystal and therefore preserve complete metamorphic records (see Section 6.1).

4.1. Garnet

The garnet grains are 2–3 mm in diameter and exhibit a corroded morphology with well-developed coronas of plagioclase, minor orthopyroxene, hornblende, biotite and ilmenite (Fig. 3b-f). They display obvious microstructural zoning patterns with zonal distributions of frozen mineral inclusions: (1) a diablastic core crowded with quartz, minor titanite, ilmenite, plagioclase and apatite; (2) an inclusion-poor mantle with discrete quartz, clinopyroxene, plagioclase, and rutile; and (3) a corroded rim surrounded by corona/symplectite layers consisting of plagioclase + hornblende/biotite+ ilmenite in the inner layer and plagioclase + orthopyroxene in the outer layer (Fig. 3c-f). In the collected samples, a few garnets were completely consumed, with only pseudomorphs remaining. It must be mentioned that those inclusions surrounded by crack coalescence with the matrix are excluded to avoid secondary origin or breakdown products of the host garnets.

Three representative garnet grains share similar compositional profiles; here, we only take one as an example to illustrate their chemical zoning patterns (the other two profiles are not shown here). The garnet in the examined sample was dominated by almandine, grossular and pyrope, with minor amounts of spessartine (Table 1) ($X_{Alm} = Fe^{2+}/(Ca + Fe^{2+} + Mg + Mn)$, $X_{Grs} = Ca/(Ca + Fe^{2+} + Mg + Mn)$, $X_{Pyr} = Mg/(Ca + Fe^{2+} + Mg + Mn)$ and $X_{Sps} = Mn/(Ca + Fe^{2+} + Mg + Mn)$). Compositional mapping illustrates that the garnet exhibits obvious compositional zoning (Fig. 4). A representative compositional profile is shown in Fig. 5. Accordingly, the garnet is artificially divided into core, mantle and resorbed rims (cf. Fig. 5a & b). The X_{Pyr} displays a slightly increasing trend in the core (0.07 → 0.10), a dramatic increase trend in the mantle (0.10 → 0.16), and a decreasing trend in the rim (0.16 → 0.14). The X_{Grs} exhibits a pronounced trend of rimward increase from the core to the core-mantle boundary (0.29 → 0.37) and then decreases from the mantle (0.37 → 0.30) to the resorbed rim (0.30 → 0.22). The Fe# index [$= Fe^{2+}/(Fe^{2+}+Mg)$] exhibits a small decreasing trend in the core (0.89 → 0.85), an obvious decrease in the mantle (0.85 → 0.77), and an increasing trend toward the rim (0.77 → 0.81). The X_{Alm} decreases slightly in the core (0.57 → 0.52) and then increases toward the rim (0.52 → 0.61). The X_{Sps} exhibits a 'bell-shaped' pattern from the core to mantle (0.09 → 0.01), with rimward resorption (0.01 → 0.02).

4.2. Other minerals

Clinopyroxene mainly occurs as porphyroblasts with lengths of up to 4 mm in the studied samples (Fig. 3c-d, g-h). It typically displays retrogressed textures as intergrowth of plagioclase + diopsidic clinopyroxene ± amphibole ± orthopyroxene ± quartz (Fig. 3 c-d, g-h). Area analyses of selected grains with the intergrowth of plagioclase + diopsidic clinopyroxene ± orthopyroxene ± quartz were undertaken

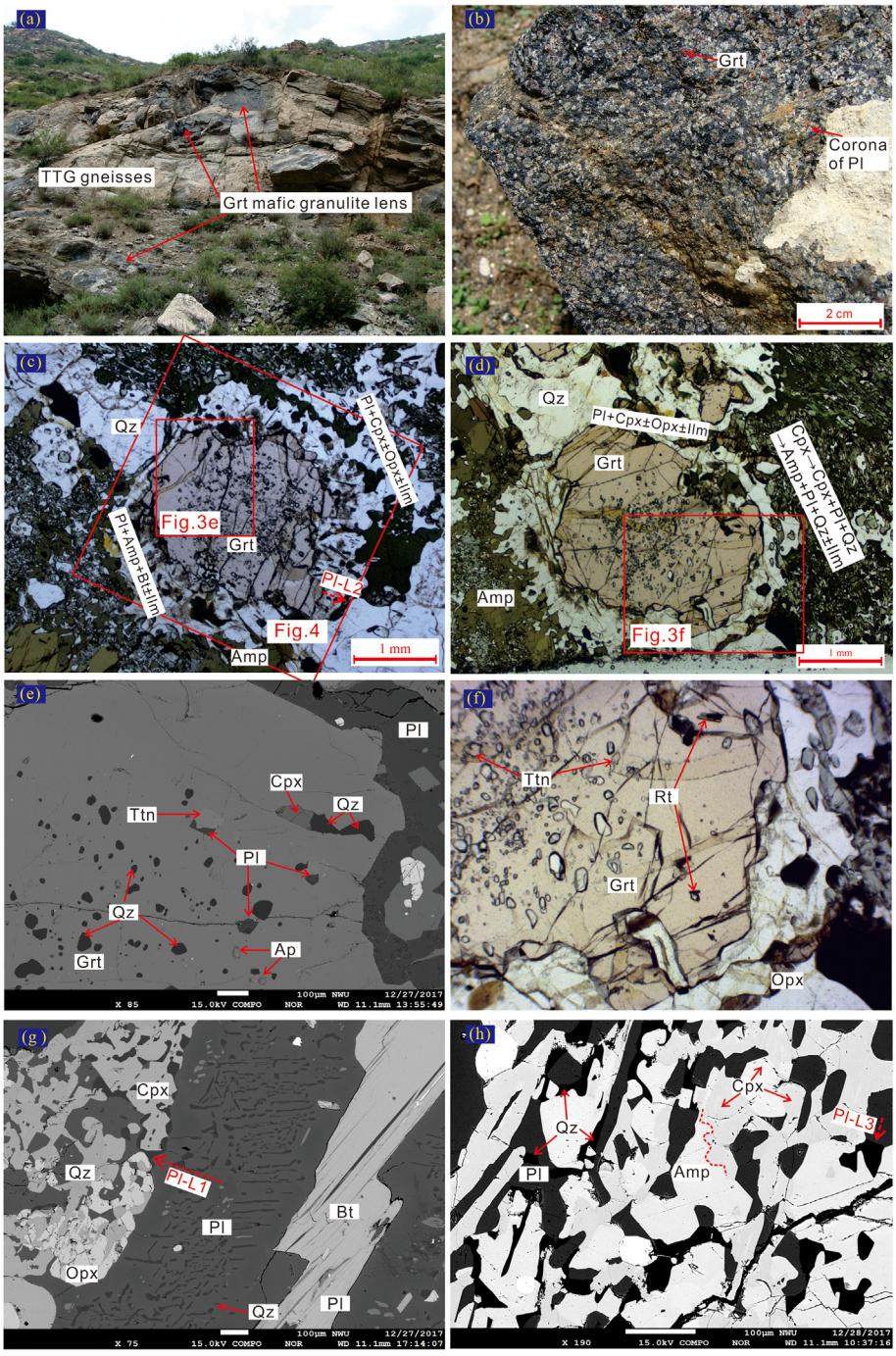

Fig. 3. Representative field photographs and photomicrographs of garnet mafic granulites from northern Hengshan area, the NCC. (a) The mafic high-pressure granulites occur as lenses in the TTG gneisses, (b) close up of sample 17BM5, (c-d) microstructures of studied garnet mafic granulites. A composition profile (Pl-L2) of corona-type plagioclase is shown in Fig. 3c. Note the garnet and clinopyroxene decomposition textures, see the text in detail, (e-f) close up of mineral inclusions in the local domains of the garnets in Fig. 3c-d, note that rutile and titanite are included in mantle and core of the garnet in Fig. 3f, respectively, (g) subhedral plagiocalse in matrix with some exsolved quartz lamina, and a composition profile (Pl-L1) is shown, (h) close up of intergrowth of secondary diopsidic clinopyroxene + hornblende ± orthopyroxene ± quartz after precursor clinopyroxene porphyroblasts. A composition profile (Pl-L3) of symplectic plagioclase included in porphyroblastic clinopyroxene is shown. Mineral abbreviations after Whitney and Evans (2010): Amp-amphiboble, Bt-biotite, Cpx-Clinopyroxene, Grt-garnet, Opx-orthopyroxene, Pl-plagioclase, Qz-quartz, Rt-rutile, Ttn-titanite, Ilm-ilmenite.

to reintegrate the original composition of clinopyroxene before breakdown. The results showed that the precursor clinopyroxene had jadeite contents of 0.22–0.27 (Table 1). The secondary diopsidic clinopyroxene and clinopyroxene inclusions in garnet display very low jadeite contents of ~0.01 (Table 1). Most of the secondary diopsidic clinopyroxene grains were replaced by amphibole + plagioclase ± quartz (Fig. 3h). Orthopyroxenes occur as retrograde grains adjacent to or included in the porphyroblastic clinopyroxene (Fig. 3c-d, f, h).

Plagioclase has three major occurrences: (1) inclusions in garnet, sometimes accompanied by titanite and quartz (Fig. 3e); (2) porphyroblasts/subidioblastic laths (up to 2.5 mm) in the matrix, with many exsolved quartz rods in the cores and a clean rim (Fig. 3g); and (3) coronas around garnets (Fig. 3c-f) or intergrowth with diopsidic clinopyroxene, amphibole and quartz after the original clinopyroxene porphyroblasts (Fig. 3g, h). A plagioclase porphyroblast shows a rimward increasing X_{An} (0.21 → 0.36, Fig. 6a), which is similar to the

Table 1
Representative mineral compositions for sample 17BM5.

Mineral	garnet L1: rim→mantle→core→mantle→rim							Plagioclase					Clinopyroxene			opx	Amp
analyses	L1–01	L1–03 (P2)	L1–08 (P1)	L1–25 (P0)	L1–42 (Q1)	L1–48 (Q2)	L1–50	pl-inc	pl-c	pl-r	pl-s	pl-cor	cpx-inc	cpx in matrix	cpx-reint		
SiO_2	38.18	38.20	37.65	37.27	38.03	38.29	37.33	56.73	62.89	59.13	60.09	57.53	51.94	51.79	55.94	50.19	42.54
TiO_2	0.05	0.05	0.02	0.13	0.02	0.11	0.00	0.10	0.00	0.00	0.00	0.00	0.07	0.02	0.28	0.08	1.93
Al_2O_3	20.86	20.97	20.90	20.53	20.83	20.83	21.12	27.09	22.86	25.25	24.72	26.38	1.65	1.00	6.41	0.49	11.58
FeO(T)	28.29	26.50	24.99	25.49	24.74	26.87	27.06	0.39	0.10	0.21	0.31	0.28	12.00	13.52	8.94	33.56	19.21
MnO	1.03	0.55	1.52	3.93	0.88	0.25	0.74	0.03	0.05	0.02	0.00	0.00	0.10	0.18	0.00	0.61	0.08
MgO	3.72	3.94	2.47	1.73	2.11	4.15	3.43	0.01	0.00	0.01	0.00	0.00	11.60	11.11	10.42	14.57	7.98
CaO	7.77	10.50	12.36	10.37	13.19	10.24	9.69	9.15	4.47	7.28	6.56	8.82	22.51	22.37	15.05	0.53	10.98
Na_2O	0.01	0.00	0.01	0.02	0.02	0.04	0.01	6.25	8.80	7.09	7.45	5.31	0.17	0.18	2.73	0.01	1.52
K_2O	0.00	0.00	0.00	0.00	0.00	0.00	0.00	0.37	0.48	0.24	0.32	0.27	0.00	0.00	0.00	0.03	1.16
Total	99.92	100.71	99.92	99.47	99.80	100.79	99.38	100.12	99.64	99.22	99.44	98.60	100.03	100.16	99.77	100.08	96.99
Si	3.02	2.98	2.97	2.98	3.00	2.98	2.96	2.55	2.79	2.66	2.69	2.60	1.96	1.97	2.07	1.97	6.50
Ti	0.00	0.00	0.00	0.01	0.00	0.01	0.00	0.00	0.00	0.00	0.00	0.00	0.00	0.00	0.01	0.00	0.22
Al	1.94	1.93	1.94	1.94	1.94	1.91	1.97	1.44	1.20	1.34	1.30	1.41	0.07	0.04	0.28	0.02	2.09
Fe^{2+}	1.85	1.62	1.54	1.63	1.58	1.63	1.69	0.00			0.00	0.01	0.37	0.40	0.28	1.08	2.40
Fe^{3+}	0.02	0.12	0.12	0.08	0.06	0.13	0.12	0.01	0.00	0.01	0.01	0.00	0.01	0.03	0.00	0.03	0.06
Mn	0.07	0.04	0.10	0.27	0.06	0.02	0.05	0.00	0.00	0.00	0.00	0.00	0.00	0.01	0.00	0.02	0.01
Mg	0.44	0.46	0.29	0.21	0.25	0.48	0.40	0.00	0.00	0.00	0.00	0.43	0.65	0.63	0.58	0.85	1.82
Ca	0.66	0.88	1.04	0.89	1.12	0.85	0.82	0.44	0.21	0.35	0.31	0.47	0.91	0.91	0.60	0.02	1.80
Na	0.00	0.00	0.00	0.00	0.00	0.01	0.00	0.54	0.76	0.62	0.65	0.02	0.01	0.01	0.20	0.00	0.45
K	0.00	0.00	0.00	0.00	0.00	0.00	0.00	0.02	0.03	0.01	0.02		0.00	0.00	0.00	0.00	0.23
													4.00				
Xsps	0.02	0.01	0.03	0.09	0.02	0.01	0.02	Ab 0.54	0.76	0.63	0.66	0.51	Wo 0.47	0.47			
X_{alm}	0.61	0.54	0.52	0.54	0.53	0.55	0.57	An 0.44	0.21	0.36	0.32	0.47	En 0.34	0.33			
X_{pyr}	0.15	0.15	0.10	0.07	0.08	0.16	0.14	Or 0.02	0.03	0.01	0.02	0.02	Fs 0.19	0.20			
X_{grs}	0.22	0.29	0.35	0.30	0.37	0.29	0.28						Jd 0.01	0.01	0.25		
Fe#	0.81	0.78	0.84	0.89	0.86	0.77	0.81						0.64	0.61	0.67	0.44	0.43

pl-inc - inclusion of garnet, pl-c & pl-r - core and rim of plagioclase in matrix, pl-cor - plagiocalse corona around garnet. Cpx-inc - clinopyroxene inclusion in garnet, cpx-reint- re-integrated clinopyroxene. Fe^{3+} is calculated by stoichiometric charge balance. Xsps = [Mn/(Mn + Ca + Mg + Fe^{2+})], Xalm = [Fe^{2+}/(Mn + Ca + Mg + Fe^{2+})], Xpyr = [Mg/(Mn + Ca + Mg + Fe^{2+})], Xgrs = [Ca/(Mn + Ca + Mg + Fe^{2+})], Fe# = Fe^{2+}/(Fe^{2+}+Mg). Xan = Ca/(Ca + Na + K), Xab = Na/(Ca + Na + K), Xor = K/(Ca + Na + K). Xwo = Ca/(Ca + Mg + Fe^{2+}), Xen = Mg/(Ca + Mg + Fe^{2+}), Xfs = Fe^{2+}/(Ca + Mg + Fe^{2+}), Xjd = Na/(Na + Ca).

plagioclase profile of Sample A12 (see Fig. 6a in Zhao et al., 2001). A plagicolcase corona displays a decreasing trend from the garnet rim to core (X_{An} = 0.63 → 0.43, Fig. 6b). The symplectic plagioclase included in the porphyroblastic clinopyroxene shows an inrease in X_{An} from core to rim (0.28 → 0.40, Fig. 6c).

Amphibole mainly has three habits: porphyroblasts with pseudomorphs of precursor clinopyroxene; flakes together with secondary diopsidic clinopyroxene, plagioclase, quartz, and orthopyroxene after precursor clinopyroxene porphyroblasts (Fig. 3h); or as symplectic minerals together with plagioclase near garnet rims (Fig. 3c, d). No significant compositional variations were observed in the amphibole grains. Biotites are locally and heterogeneously distributed in matrix domains with intensive retrogression or as scarce flakes near resorbed garnet rims (Fig. 3c, d).

Quartz grains occur either as inclusions within garnet cores or as matrix minerals (Fig. 3c-f). Titanites occur in the core to the core-mantle boundary of garnet (Fig. 3e, f). Ilmenites occur as trace inclusions in the garnet core or as retrograde products after the decomposition of the garnet rims (Fig. 3c). Rutiles occur as mineral inclusions in the mantle and rim of the garnet (Fig. 3f) and in the matrix.

4.3. Metamorphic mineral assemblage evolution

Based on the above microstructure and mineral composition variations, the metamorphic evolution of the investigated sample was probably divided into early prograde (M_{1-1}), late prograde (M_{1-2}), near peak (M_{2-1}), peak (M_{2-2}), decompression (M_3) and cooling (M_4) metamorphic stages. The early prograde stage (M_{1-1}) features poikilitic garnet cores (P_0 in Fig. 5) and their inclusions, with maximum X_{Sps} and Fe# and minimum X_{Pyr}. The possible mineral assemblages are garnet core–clinopyroxene–quartz–titanite–plagioclase–ilmenite ± amphibole. The late prograde stage (M_{1-2}) is characterized by inclusion-type mineral assemblages in the core-mantle boundary of garnet (P_1/Q_1 in Fig. 5). This occurs with increasing X_{Grs} up to its maximum and the inflection points of Fe# and X_{Pyr}. The near-peak stage (M_{2-1}) features the occurrence of rutile in the garnet mantle, rim and matrix, corresponding to the presently preserved maximum of X_{Pyr} and minimum of Fe# in the garnet (P_2/Q_2 in Fig. 5). The possible mineral assemblages are garnet– clinopyroxene–plagioclase–rutile–quartz ± amphibole. The peak metamorphic assemblages (M_{2-2}) should have been recorded in the original garnet rim, but the domains have broken down into other minerals and their original information is destroyed. The decompression stage (M_3) is characterized by the breakdown of garnet into plagioclase and pyroxene and the breakdown of clinopyroxene porphyroblast into diopsidic clinopyroxene and plagioclase bleb, with rare orthopyroxene. The M_4 cooling stage represents retrogression of amphibolite facies with assemblages of clinopyroxene–plagioclase–amphibole–biotite–ilmenite. These four generations of assemblages define a clockwise *P-T* path.

5. Results

5.1. Geothermobarometries

Owing to the rare relict inclusion-type mineral assemblages in garnet and intensive breakdown of garnet rims and precursor clinopyroxene porphyroblasts, no suitable geothermobarometries could be applied to calculate the conditions for M_{1-1}, M_{2-1} and M_{2-2}. The *P-T* conditions of M_{1-2} are estimated at 8–9.5 kbar/635–690 °C using the garnet-clinopyroxene geothermometers of Powell (1985)

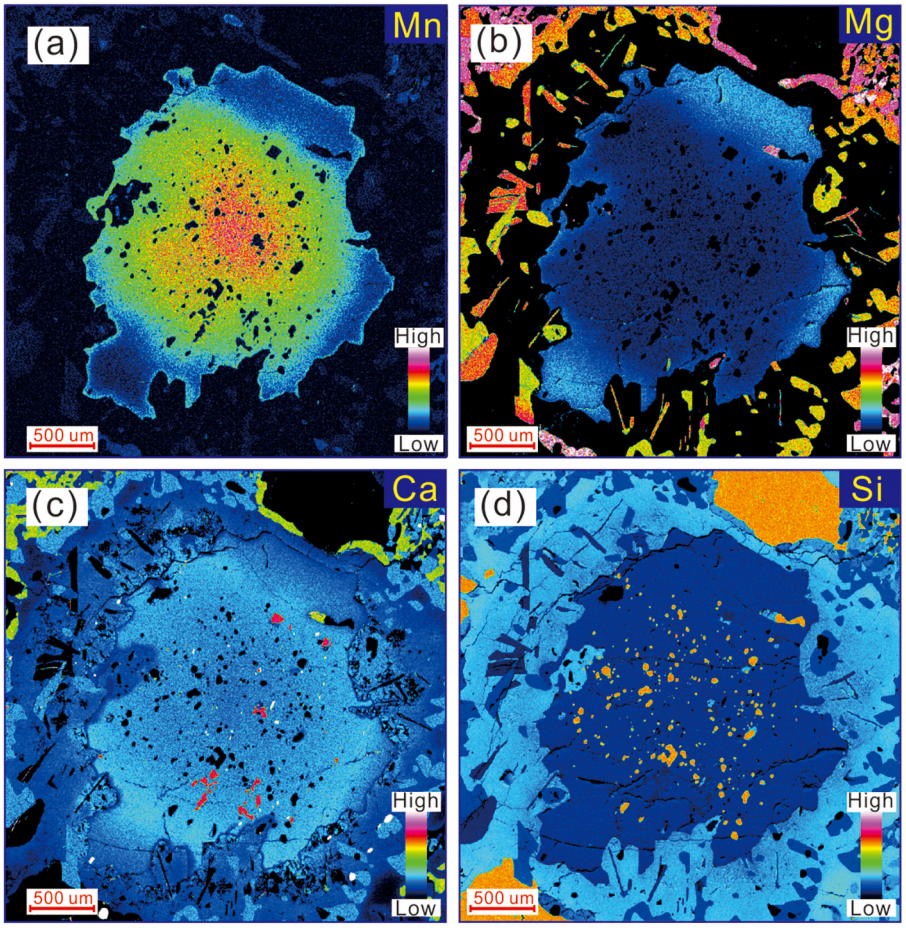

Fig. 4. Compositional maps of Mn, Mg, Ca, Si of a garnet in the Sample 17BM5.

and Ravna (2000) and the garnet–clinopyroxene– plagioclase– quartz geobarometers of Newton and Perkins (1982) and Eckert Jr. et al. (1991), based on inclusion-type mineral compositions in the core-mantle boundary of garnet (see Fig. 5b). The metamorphic conditions of M_3 are estimated at 8.5–10.5 kbar/ 820–838 °C using garnet-orthopyroxene-plagiocalse-quartz thermobarometries of Lal (1993) and Bhattacharya et al. (1991). The *P-T* conditions of M_4 are estimated to be approximately 3–5 kbar/650–680 °C using hornblende-plagioclase thermometer of Holland and Blundy (1994) and hornblende-plagioclase-quartz barometer of Bhadra and Bhattacharya (2007).

5.2. Phase equilibrium modeling

P-T pseudosections were calculated using THERMOCALC version 3.45 (Powell and Holland, 1988 and updates) and an internally consistent dataset (ds62, Holland and Powell, 2011). The system with components Na_2O-CaO-FeO-MgO-Al_2O_3-SiO_2-H_2O-TiO_2-O (NCFMASHTO) was chosen to approximate the studied mafic granulite. MnO was not included because it cannot currently be modelled for metabasic rocks (Green et al., 2016). K_2O was ignored here because of (1) low proportions of K-rich minerals (e.g., <2% biotite) in the investigated sample, (2) most of the K-rich minerals in the matrix might be produced by retrograde K-bearing crustal fluids, as they are mainly distributed in domains with intensive retrogression, and (3) its insignificant influence on the major phase relationships under high *P-T* conditions. The phases involved in the thermodynamic modeling and corresponding A-X relationships are silicate melt, augitic clinopyroxene and hornblende (Green et al., 2016), plagioclase (Holland and Powell, 2003), garnet, ilmenite and orthopyroxene (White et al., 2014). Rutile, titanite, albite, H_2O, and quartz are the pure phases.

The bulk rock compositions of the sample in weight percent are SiO_2 (48.93), TiO_2 (1.51), Al_2O_3 (14.13), Fe_2O_3(T) (16.13), MnO (0.24), MgO (5.73), CaO (9.42), Na_2O (2.27), K_2O (1.02), and P_2O_5 (0.19). Before modeling, several prior adjustments to the bulk composition were performed: (1) the content of CaO was after the extraction of CaO in apatite; (2) the proportion of ferric iron was arbitrarily assumed to be 8 mol% of total Fe; and (3) the content of water is estimated using the *P-M*(H_2O) pseudosection at an average late prograde (M_{1-2}) temperature of 660 °C. In this context, the expected *M*(H_2O) was estimated to be 4.08–5.326 (X = 0.4–0.54), which is constrained by the late prograde mineral assemblage and the estimated pressures of 8–9.5 kbar (white area in Fig. 7a). Therefore, the water content was chosen as the average *M*(H_2O) = 4.703 mol% (X = 0.47 mol%) in Fig. 7a, and the new bulk composition of the component system in mole percent was H_2O: SiO_2: Al_2O_3: CaO: MgO: FeO: Na_2O: TiO_2: O = 4.703: 50.930: 8.665: 10.222: 8.883: 12.621: 2.290: 1.180: 0.506. Furthermore, in this modeling, a fixed bulk rock composition was used. The effect of garnet core fractionation is not considered, because the garnet core only accounts for a minor volume of the entire garnet, which has less effect on the modelled *P-T* pseudosection (e.g., Zhang et al., 2020a).

The *P-T* pseudosection was calculated in the range of 4–20 kbar and 600–900 °C (Fig. 7b). In the diagram, garnet forms at 6–7 kbar, and melt appears at 670–770 °C. The stability of plagioclase varies from 10 to 17 kbar with increasing temperature. The hornblende boundary line has a negative slope from 750 to 900 °C at a relatively high pressure. The appearance of orthopyroxene and disappearance of quartz occur under low-pressure/high-temperature conditions. H_2O is in excess in the *P-T*

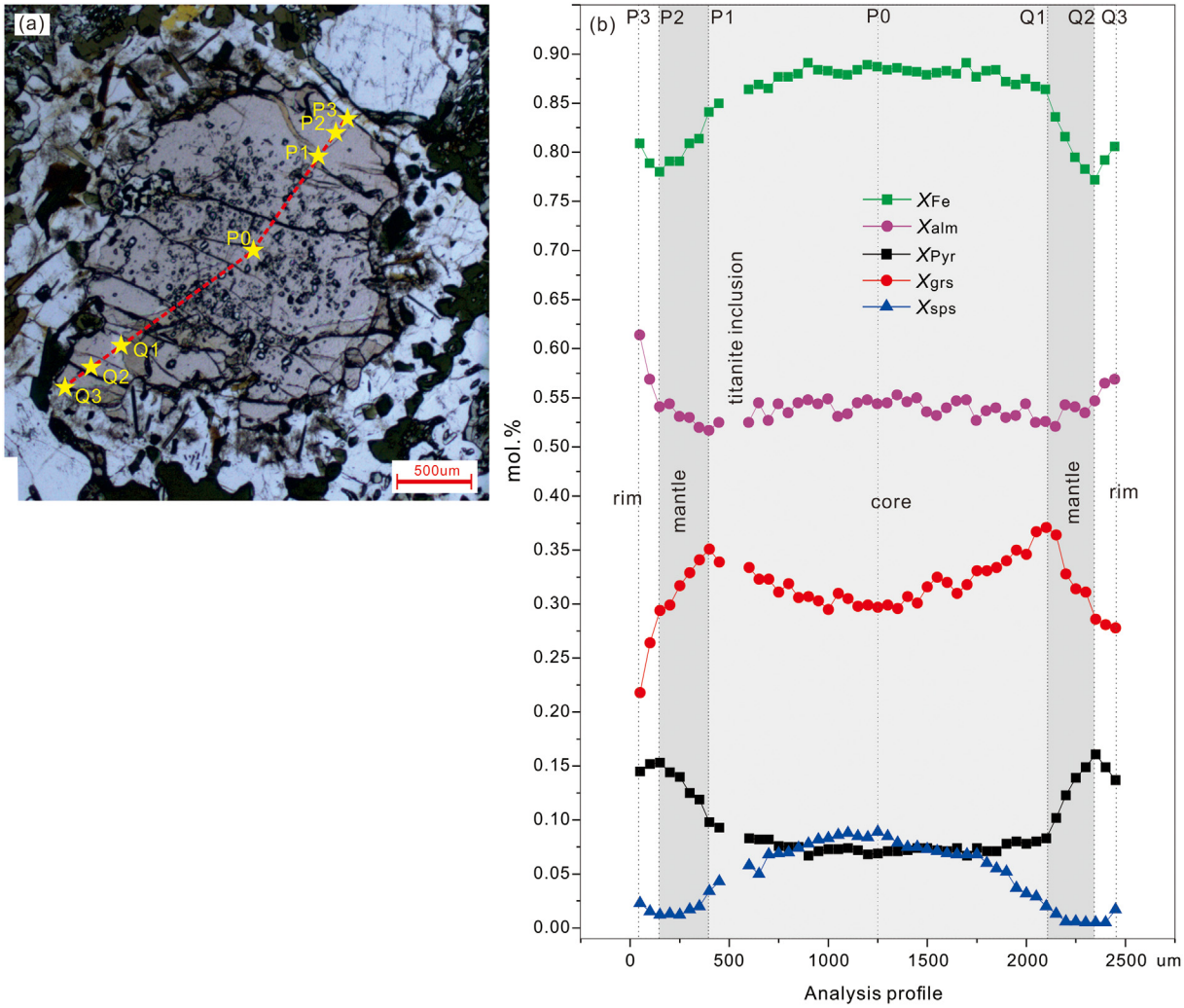

Fig. 5. A representative compositional profile of garnet in the sample 17BM5.

range of >11.6 kbar/<700 °C and < 6.6 kbar/625–760 °C. The proportions of titanium-bearing minerals (ilmenite, titanite and rutile) were variable and correlated. Rutile is stable at higher pressures and exhibits a decreasing trend from 17 to 10 kbar with increasing temperature. Ilmenite is stable at pressures below 11 kbar, while titanite is stable at relatively low temperatures below 800 °C with pressures of 7–17 kbar. This correlation suggests that rutile becomes stable at the expense of titanite in the *P-T* range of ~10–17 kbar/<785 °C and at the expense of ilmenite at ~10.4–11.2 kbar/> 785 °C.

The modelled Fe# isopleths of garnet have slightly positive to negative slopes and decrease with increasing temperature, which suggests that they are useful indicators of temperatures. Specifically, the lower the Fe#, the higher the temperature (Fig. 8a). The X_{Grs} isopleths are complex with several saddle points in the *P-T* space and vary with

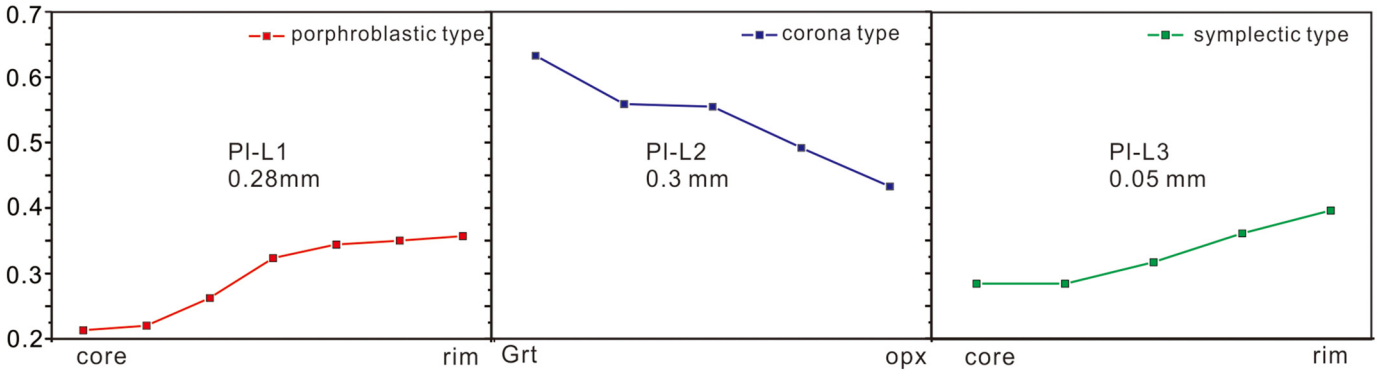

Fig. 6. X_{An} profiles of different type plagioclase grains in Sample 17BM5. (a) Pl-L1, porphyroblastic plagioclase zoning, (b) Pl-L2, corona-type plagioclase zoning, (c) Pl-L3, symplectic plagioclase after porphyroblastic clinopyroxene.

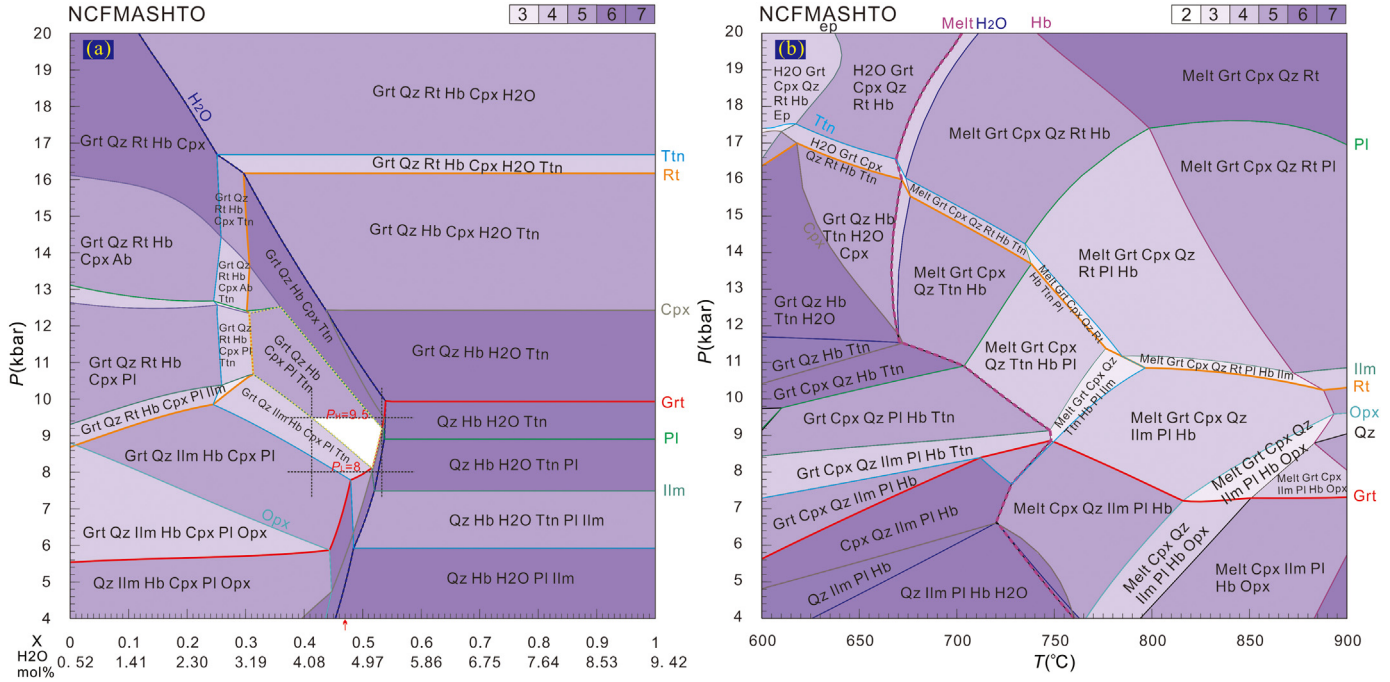

Fig. 7. (a) *P-M*(H_2O) pseudosection at 660 °C. The x axis ranges from *M*(H_2O) = 0.52 mol% at *X* = 0, and *M*(H_2O) = 9.42 mol% at *X* = 1. The confined white area represents *P-X* space of late prograde assemblage (Grt-Qz-Hbl-Cpx-Pl-Ttn) at *T* = 660 °C, *pH* = 9.5 kbar, P_L = 8 kbar, (b) *P-T* pseudosection at *M*(H_2O) = 4.703 mol%.

mineral assemblages (Fig. 8a). The garnet modal proportions increase with pressure or temperature, indicating that they are sensitive to changes in physical conditions: the higher the pressure or temperature, the greater the proportion of garnet (Fig. 8b). The contours of the quartz modal proportion form a semicircle with a center at 8–13 kbar/600–750 °C and decreases outward in *P-T* space, which suggests that the quartz proportion could serve here as an approximate *P-T* indicator above 600–750 °C: the higher the metamorphic conditions are, the lower the proportion of quartz (Fig. 8b).

The *P-T* conditions of the early prograde stage (M_{1-1}) were estimated to be ~6–9 kbar/600–700 °C with an average of 7.5 kbar/650 °C, based on the intersection of Fe# and X_{Grs} in the garnet core (P_0). The estimated *P–T* conditions are located in the garnet initially growth zone, with a mineral assemblage of Grt–Cpx–Qz–Ilm–Pl–Hbl (Fig. 8). The

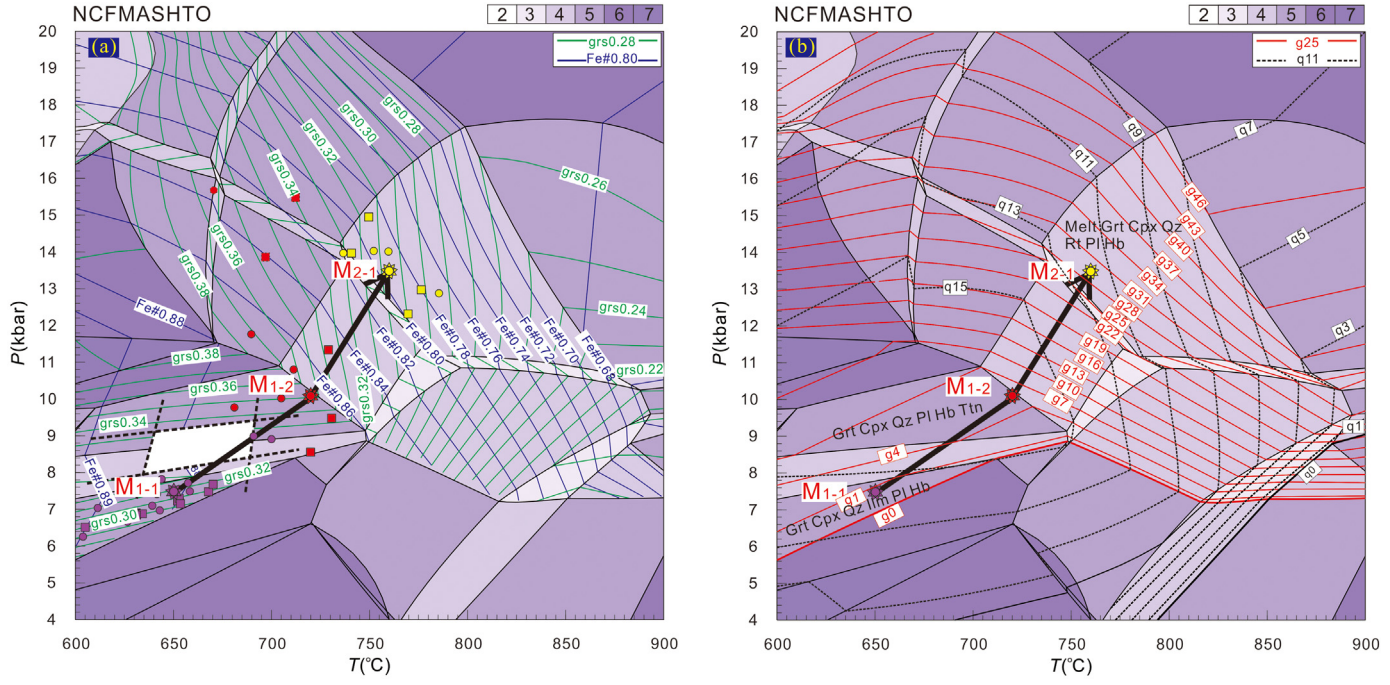

Fig. 8. (a) Isopleths of X_{Grs} and Fe# in garnet, and plots of composition analyses in the *P-T* space. Squares and circles represent analyses in the left and right of the profile, and star represent average *P*, *T* values. Purple, red and yellow represent analyses of the garnet inner core, core-mantle boundary, and inner rim respectively. Four analyses in the plagioclase-absent field are neglected, which might be related to analytical error or roughness of chosen analysis spot/area. An inferred prograde *P-T* segment is shown using garnet compositions from core to mantle. The late prograde *P-T* conditions derived from thermobarometries are also shown in a white quadrangle. (b) Modal proportions of garnet and quartz, as well as the inferred prograde *P-T* segment are shown. (For interpretation of the references to colour in this figure legend, the reader is referred to the web version of this article.)

late prograde stage M_{1-2} was metamorphosed at ~9–11.2 kbar/680–740 °C, with an average of 10.1 kbar/720 °C, extracted from the intersection of maximum X_{Grs} and corresponding Fe# (P_1/Q_1), where the X_{Grs} isopleths display a saddle point at the maximum (Fig. 8a). They were in the stability field of Grt–Cpx–Qz–Pl–Hbl–Ttn. Crossing this point, the X_{Grs} began to decrease. The *P-T* conditions of the near-peak pressure stage (M_{2-1}) were estimated to be ~12–15 kbar/735–785 °C with an average of 13.5 kbar/760 °C, based on the minimum of Fe# and corresponding X_{Grs} of the garnet mantle (P_2/Q_2). They lie in the rutile stability field without titanite and ilmenite, and its corresponding mineral assemblage is Grt–Cpx–Qz–Pl–Hbl–Rt (Fig. 8). The metamorphic conditions of the peak stage (M_{2-2}) were estimated to be >13.5 kbar/ >760 °C based on increasing garnet volumes. The *P-T* conditions of the decompression (M_3) and cooling (M_4) stages were approximately 7–10 kbar/>800 °C and < 720 °C, respectively, based on the occurrence of orthopyroxene and melt.

6. Discussion

6.1. Zoned garnet as a recorder of granulite-facies metamorphic processes

As a versatile mineral in metamorphic rocks, garnet appears to be a brilliant pearl of metamorphic petrology. It records many tectono-metamorphic information on the determination and characterization of a *P-T-t* path. Garnets often develop variable zoning patterns, such as textural zoning with regular zonal distribution of inclusion-type minerals (e.g., Parkinson, 2000), as well as compositional zoning (e.g., Caddick and Kohn, 2013). The latter is shown not only in major elements but also in trace elements, such as Y, Sc, Cr, V, Ti and heavy rare earth elements (HREEs) (e.g., Gaidies et al., 2020; Rubatto et al., 2020), P and oxygen isotopes (e.g., Higashino et al., 2019). These zoning patterns are often preserved very well in low- to moderate-temperature metamorphic rocks (e.g., Gaidies et al., 2020; Spear, 1993).

For granulite-facies rocks, garnets often display relatively homogeneous compositional profiles for major elements due to fast diffusion rates at high temperatures (e.g., Spear, 1993); however, a few exceptions still exist, such as the garnet from ultrahigh-temperature rocks in NW Scotland (Hollis et al., 2006). Recent studies suggest that granulitic garnet can preserve obvious textural zoning and trace element zoning, even though there is a lack of major element zoning (e.g., Wu et al., 2018b; Rubatto et al., 2020; Higashino et al., 2019). For example, garnets in pelitic granulites from the Huai'an area, NCC, display relatively homogeneous X_{Sps}, X_{Alm}, X_{Pyr} and X_{Grs} profiles, except for weak zonation at the rims (Wu et al., 2016). However, the inclusions in garnet display obvious microstructural zoning with regular distribution patterns: (1) crowded quartz inclusions in the core, (2) minor kyanite–K–feldspar–bearing assemblages in the mantle, and (3) sillimanite-bearing assemblages in the rim (Wu et al., 2016, 2017, 2018b, 2019). REE profiles reveal that the HREEs decrease traveling from the core to the rim and exhibit bell-shaped zoning (Fig. 6 of Wu et al., 2017). Such textural and trace element zoning patterns suggest that the granulitic garnet could serve as a pressure and temperature resistant container that documented multiple generations of growth history from early prograde to peak metamorphic stages (e.g., Rubatto et al., 2020), while the minerals in the matrix only documented the intensive re-equilibriation at peak metamorphism, having the same assemblages as the inclusions included in the garnet rim (Wu et al., 2016, 2017, 2018b).

Fortunately, garnet grains from the studied mafic granulites preserve not only well-developed microstructural zoning but also compositional zoning. Among these, the largest garnet grain groups with pronounced zoning patterns were used to decipher the metamorphic history of the host rocks. These grains are expected to (1) illustrate the zonal distribution of multi-generation inclusion-type mineral assemblages through the center of garnet grains, (2) may preserve original composition profiles, and (3) are less modified by diffusion than the smaller grains; consequently, have more complete records from early to late metamorphic stages (e.g., Caddick et al., 2010; Gaidies et al., 2008; Wu et al., 2016, 2017, 2018b).

6.1.1. Prograde garnet behavior

The garnets in the investigated mafic granulites display well-developed microstructural zoning during progressive metamorphism. This is demonstrated by inclusion-zoned patterns with poikilitic cores crowded with quartz and sparse inclusions in mantles/rims. However, it is unfortunate that the textural zonation of granulitic garnet was not given more consideration in previous studies. At the moment of initial growth, the garnet usually encloses some superfluous or inert minerals, such as quartz and plagioclase at reaction frontiers, and protects them isolated from the matrix; they then become frozen-in mineral inclusion assemblages. The crowded quartz grains in the investigated garnet cores suggest that there were many quartz grains in the matrix during the first garnet growth. The pseudosection modeling results suggest that the largest amounts of quartz appear at 8–13 kbar/ <750 °C (Fig. 8b), which is expected to be the suitable *P-T* range for garnet to entrap many quartz grains, and agrees well with the estimated conditions of progressive M_{1-1} to M_{1-2}. As metamorphic reactions proceed with increasing temperature, the reaction and nutrient transport rates increase greatly, and the quartz proportions in the matrix decrease. Therefore, it yields less abundant mineral inclusions within newly formed garnet shells and finally produces fossilized microstructural zoning. In addition, the Ti-bearing mineral inclusions alternate from ilmenite and titanite to rutile from garnet cores to mantles/rims. This suggests increases in pressure and temperature (Fig. 8b).

Meanwhile, significant compositional variations were produced with varying metamorphic mineral assemblages during prograde metamorphism. These variations are illustrated here as typical bell-shaped X_{Sps} zoning, initially slightly flat and then increasing or decreasing X_{Pyr} and Fe#, and initially increasing and finally decreasing X_{Grs} outward from garnet core to mantle, which suggests that the garnet grows with increasing metamorphic conditions from ~7.5 kbar/~650 °C (early prograde stage), ~10.1 kbar/~720 °C (late prograde stage) ~13.5 kbar/~760 °C (near-peak stage) to higher *P-T* conditions. The results agree with the records from the microstructural zoning, and are somewhat similar to those reported by Zhang et al. (2018). As shown in Fig. 6 of Zhang et al. (2018), it is suggested that garnet grows outside of plagioclase stability, which contradicts the petrological observation that plagioclase is included in garnet and can not reasonably explain the initially increasing X_{Grs} pattern from the core to the core-mantle boundary (0.3 → 0.35/0.37). This is probably related to the unsuitable A-X relationships for the mafic granulites in questions in Zhang et al. (2018). In addition, the results suggest that the maximum of X_{Grs} in garnet does not necessarily form at the peak-pressure metamorphic stage as early thought (e.g., Zhao et al., 2001). In this regard, it is helpful to judge equilibrium mineral pairs for using geothermobarometers (e.g., Cooke et al., 2000). This indicates that the assumed equilibrium compositions using the core of garnet, sodic plagioclase, and clinopyroxene in Zhao et al. (2001) are not in equilibrium at the high-pressure granulite-facies stage. Therefore, their yielding conditions (13.4–15.5 kbar/770–840 °C) of the high-pressure granulite-facies stage require re-calculation.

The prograde metamorphism of the high-pressure mafic granulites from the study area is similar to that in rocks from the Huai'an area, approximately 300 km north of the study area (Guo et al., 2002; Wu et al., 2018a). Wu et al. (2018a) identified some robust petrologic indicators, including (1) the presence of quartz, titanite and high-aluminum diopside in garnet cores and mantles but their absence in the matrix, and (2) bell-shaped X_{Sps} and increasing X_{Pyr} from garnet cores to mantles. The development of garnet zoning patterns thus suggests that high-pressure mafic granulites from the north-central part of the NCC underwent Paleoproterozoic burial processes with increasing pressure and temperature before peak metamorphism.

6.1.2. Retrograde metamorphism and its influence on peak metamorphic records

Garnet grains from regional amphibolite, granulite or eclogite terranes often develop variable reaction microstructures, such as coronas and symplectites, in response to decompression during exhumation processes. In the studied mafic granulites, garnet grains displayed variable resorption textures. Some garnet grains exhibit two layers of symplectites/coronas, with plagioclase + amphibole/biotite near garnet and plagioclase + clinopyroxene/orthopyroxene near quartz, which suggests the following two reactions:

$$\text{Garnet} + \text{quartz} \rightarrow \text{plagioclase} + \text{orthopyroxene} + \text{clinopyroxene} \pm \text{ilmenite},$$

$$\text{Garnet} + \text{quartz} + H_2O + K^+ \rightarrow \text{plagioclase} + \text{amphibole/biotite} \pm \text{ilmenite}$$

Through such decomposition and rehydration reactions, the rim composition in the garnet is redistributed. Mn is resorbed owing to its strong preference for garnet (e.g., Fig. 5b), while Fe^{2+}, Ca and Mg are redistributed between the garnet rims and the retrograde products. The same situation holds for HREEs in garnet. For example, HREEs in garnet of mafic granulites from the Huai'an area exhibit bell-shaped patterns from core to mantle, but an obvious resportion with sharp increases near the broken rim. Therefore, the retrograde reactions not only destroyed the original rim along with the original composition.

Thermodynamic modeling results suggest that garnet often grows with increasing pressure and/or temperature (Fig. 8b). This implies that the peak metamorphic records should be preserved in a very thin rim toward the garnet surface. Figs. 9a shows the accreted garnet shells according to zoning patterns in Figs. 4 and 5, in which the rim includes two parts: the preserved present-day resorption rim and the lost rim. It also suggests that the thin rim of large garnet accounts for a large volume proportion (Table 2); In verse, the accreted thickness of the new shell is thinner if an equal volume of garnet grows, which is also helpful for interpreting Lu–Hf ages of zoned garnet (e.g., Cheng and Cao, 2013, and references therein). The results indicate that peak metamorphic information must be lost (e.g., Carlson, 2002; Spear, 2014; Zhang et al., 2018). This suggests that the retrograde garnets are unable to preserve peak metamorphic information, and previously estimated peak metamorphic *P-T* results from garnet inner rim compositions (unaffected

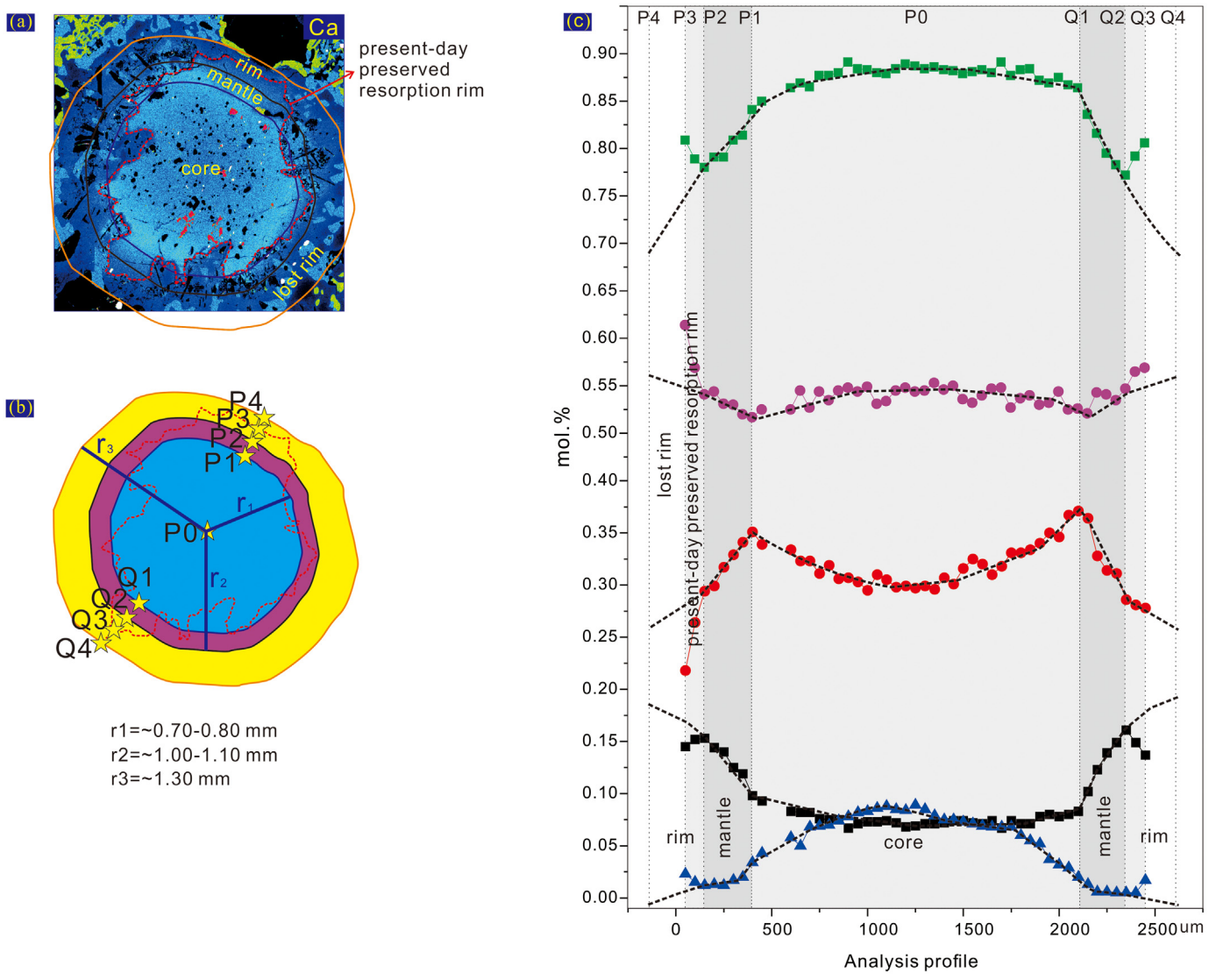

Fig. 9. (a) Reconstruction of accreted garnet shells according to Figs. 4 and 5, and the estimated original/lost rim boundary at the reaction front near clinopyroxene. The present-day preserved resorbed rim is also shown, (b) radiuses of accreted garnet shells, (c) qualitatively extrapolations of unaffected composition profiles from P_2 (Q_2) to P_4 (Q_4).

Table 2
The mode, volume proportions of the studied garnet in Fig. 4 of sample 17BM5.

Grt	Inclusions	Accumulated radius (mm)	Accumulated volume ($4/3*\pi*r^3$) (mm^3)	Accumulated Vol%	Individual Vol%	Individual thinkness of each shell (mm)	Accumulated mol. %
Core	Qz, Ttn, Ilm, Pl, Ap	~0.7–0.8	1.44–2.14	16–23	16–23	0.70–0.80	7–11
Mantle	Qz, Cpx, Pl, Rt	~1.0–1.1	4.19–5.57	46–61	23–45	0.20–0.40	21–28
rim	Rt	~1.3	9.2	100	39–54	0.20–0.30	46

Note: The original diameter is estimated at ~2.60 mm, and accumulated radiuses of core, mantle to rim are estimated at ~0.70–0.80, ~1.00–1.10 and 1.30 mm, respectively. The accumulated volumes and accumulated volume proportions, individual voulme proportion and individual thinkness of core, mantle and rim are shown in the columns 4–7, respectively. If the total model of garnet in the studied sample is assumed at ~46% based on peak conditions based on Jd in Cpx and absence of hornblende (see in Fig. 10), the accumulated modes of garnet are estimated at 7–11, 21–28 and 46 mol% for core, mantle and rim, respectively.

by resorption) are possibly lower than real conditions experienced by the host rocks, as discussed in the next section.

Accompanying the breakdown of garnet, the minerals in the matrix also suffered intensive retrogression and rehydration. For instance, the porphyroblastic clinopyroxene decomposes into diopsidic clinopyroxene, plagioclase and minor orthopyroxene. It is then replaced by amphibole, biotite and minor quartz. Therefore, the present-day minerals in the matrix are mainly breakdown products corresponding to the retrogressive granulite- (M_3) and amphibolite-facies (M_4) assemblages, respectively.

6.1.3. Reconstruction of P-T evolution

Although the peak metamorphic garnet domain is destroyed by retrograde breakdown reactions, the original information of such garnets may fortunately be restored to some degree. First, the ambiguous boundary of the lost rim could be inferred from the reaction frontier between garnet and clinopyroxene in the matrix (Fig. 9a). Therefore, original radius and total volume of the resorbed garnet can be approximately restored (Carlson, 2002; Spear, 2014). Fig. 9 shows the studied garnet in Fig. 4 as an example of accreted garnet shells during growth. It displays the radii of the accreted garnet core (r1 = ~0.70–0.80 mm), mantle (r2 = ~1.00–1.10 mm), and original rim (r3 = ~1.30 mm) using a hypothetical sphere model (Fig. 9b). The volume of each shell was calculated, as listed in Table 2. The calculation method refers to the Appendix C. Supplementary data from Wu et al. (2016). The results show that unresorbed garnet accounts for 46–61 vol% of original garnet, which suggests that the original mode is possibly in the range of 46–61 mol%, and is 1.64–2.17 times of the unresorbed garnet (~28 mol%, Fig. 8b). Here, the original garnet mode is assumed to be ~46 mol% for consistent with Jd content in Cpx and absence of hornblende in the peak assemblages (Fig. 10 and Fig. 8b). Thus, the core and mantle modes of garnet are estimated at 7–11 and 21–28 mol%, respectively, which agree well with *P-T* results of M_{1-2} and M_{2-1} yielding from composition analyses (Fig. 8b and Fig. 10).

Second, the rim composition of the precursor garnet can be estimated to some extent based on exchange and net transfer reactions and mass balance models between garnet and its surrounding minerals (Carlson, 2002; Spear, 2014). Fig. 5b shows that the composition from P_0 to P_2 (Q_2) underwent relatively insignificant modification, but the composition outward was strongly resorbed, such as the composition from P_2 (Q_2) to P_3 (Q_3). Extrapolations of unaffected composition profiles from P_2 (Q_2) to P_4 (Q_4) were qualitatively estimated, as shown in Fig. 9c (P_4/Q_4: X_{Grs} = ~0.26 & Fe# = ~0.69). In this context, the peak conditions are plausibly estimated at ~790–810 °C (Fig. 10), which is consistent with the estimated maximum temperature (797 °C, if *P* = 16 kbar, unpublished data) using the zirconium-in-rutile thermometer of Tomkins et al. (2007). They agree well with the absence or lower abundance of amphibole in the peak assemblages. The pressure of the peak metamorphic stage is not well constrained, but it might be estimated up to the transition zone of the granulite- to eclogite-facies according to a few factors: (1) the reintegrated composition of the original clinopyroxene contains jadeite contents of 0.22–0.27, which suggests that the mafic granulites documented relatively higher pressure conditions of ~15–17 kbar; (2) if the original volume of garnet (> 46 mol%) is considered, the peak pressure is possibly >15 kbar (Fig. 10); and (3) the *P-T* results should be consistent with the estimated unaffected garnet rim composition. Therefore, the estimated peak *P-T* conditions are around ~15–17 kbar/~ 790–810 °C, which are higher than the results (M_{2-1}) derived from the preserved present-day mantle-rim boundary (or inner rim) composition of garnet (P_2/Q_2, which was the closest value to the peak composition). They are also somewhat higher than previous studies by Zhao et al. (2001) and Zhang et al. (2018) (Fig. 10). The *P-T* conditions of the peak-pressure stage were overestimated in Zhao et al. (2001), in which the entrance of eclogite-facies conditions were qualitatively estimated according to a *P-T* pseudosection for a silica-saturated aluminous basalt bulk composition of Holland and Powell (1998). This model composition is higher in SiO_2 and Al_2O_3 than the studied samples in Zhao et al. (2001) and leads to the disappearance of plagioclase at higher pressures than Al_2O_3 poor basalts (Ringwood, 1975). In addition, the estimated *P-T* conditions of high-pressure granulite-facies stages are not in equilibrium using the garnet core composition, as shown by the dotted line segment in Fig. 10 (path ②).

Subsequently, the mafic granulites suffered intense decompression and garnet breakdown into plagioclase, orthopyroxene, hornblende, and ilmenite. Rutile is replaced by ilmenite at ~10.5 kbar. The *P-T* conditions of the decompression stage are roughly estimated at ~800–850 °C (Fig. 10, if *P* is assumed to be 7–10 kbar). The results are consistent with the *P-T* conditions of 8.5–10.5 kbar/820–838 °C, yielding from geothermobarometries, and from the phase equilibrium modeling of two-pyroxene granulites in the same area (see Fig. 8 of Zhang et al., 2018), which suggests that the rocks experienced near-isothermal decompression. It was then followed by cooling processes, characterized by first crossing the crystallization temperature of the melt at ~720 °C and finally undergoing subsolidus cooling to 3–5 kbar/ 650–680 °C (Fig. 10).

6.2. Tectonic significance of P-T evolution of the mafic granulites

The well-documented texturally and compositionally zoned garnet patterns provide robust petrological evidence for progressive metamorphism of the northern Hengshan mafic granulite terrane, which is a longstanding controversial issue, as stated above. Combined with coherent characteristics of deformation and metamorphism between the mafic granulites and their surrounding rocks (e.g., Kröner et al., 2006; Li et al., 1998; Zhai, 2009), it is suggested that the protoliths of these mafic granulites and their surrounding rocks must have suffered common subduction processes from the upper-middle crust to ~50 km, although no details of the subduction process are currently known.

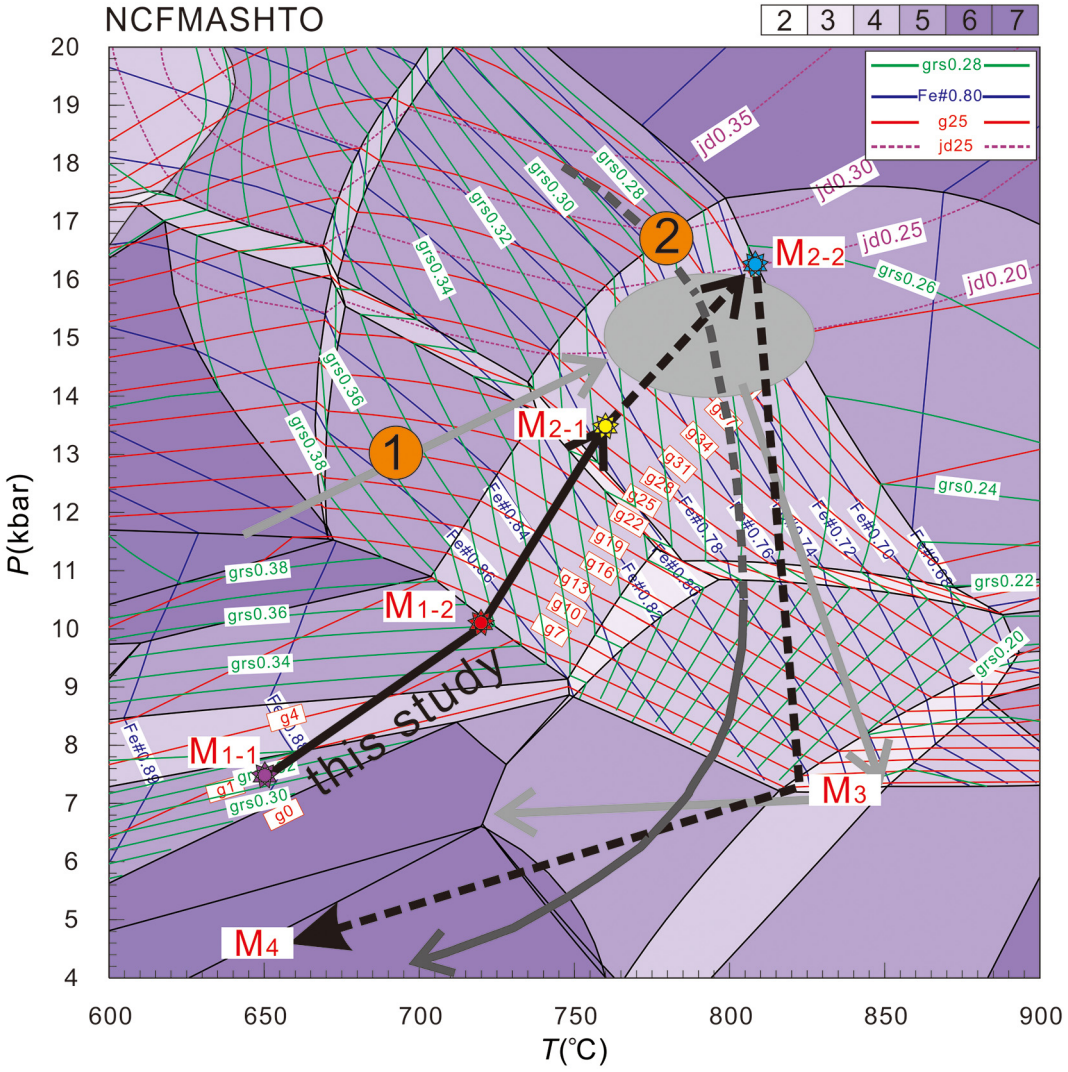

Fig. 10. Estimated peak-metamorphic conditions (blue star) and reconstruction of complete *P-T* path. The *P-T* paths of ①-Zhao et al. (2001), and ②-Zhang et al. (2018) are also shown for comparison. Dotted lines represent qualitatively estimated *P-T* segments. More discussions of the *P-T* paths see detail in text. (For interpretation of the references to colour in this figure legend, the reader is referred to the web version of this article.)

The preservation of growth zoning patterns with relatively little modifications, such as the Mn zoning in the studied garnet (except for the resorbed rim), suggests that the host rocks probably experienced a very short-lived peak metamorphic stage (e.g., Caddick et al., 2010; Chu et al., 2018; Gaidies et al., 2008; Möller, 1998; Zou et al., 2020). Furthermore, the near-isothermal decompression path suggests that the host rock must experience rapid exhumation aided by tectonic processes to the middle crust without significant thermal relaxation (e.g., Baldwin et al., 2007; Harley, 1989; Liu et al., 2017; Möller, 1998; Müller et al., 2018). Such *P-T* paths were also retrieved from other early Proterozoic high-pressure granulite and eclogite terranes, such as the Nagssugtoqidian orogen (e.g., Müller et al., 2018), the Snowbird tectonic zone (e.g., Baldwin et al., 2007), the Trans-Hudson orogen (e.g., Weller and StOnge, 2017), the Belomorian mobile belt (e.g., Liu et al., 2017), the Eburnian-Transamanzonian orogen (e.g., Loose and Schenk, 2018) and the Ubendian-Usagaran belt (e.g., Brown et al., 2020). The *E*-W trending Zhujiafang ductile shear zone might account for the exhumation of the northern Hengshan high-pressure granulite terrane (e.g., Qian et al., 2019; Wei, 2018). These results thus suggest that a relatively fast tectono-metamorphic process is involved in the formation of the Paleoproterozoic northern Hengshan high-pressure granulite terrane is preferred. They contrast with previous interpretations on metamorphic zircon U–Pb ages that the Paleoproterozoic granulite-facies metamorphism last for a long period from ~1.95 Ga to 1.85 Ga. This suggests that new interpretations on the links between metamorphism and zircon formation are urgently needed (e.g., Qian et al., 2019; Wei, 2018).

The peak metamorphic information for the mafic granulites is modified variably by retrograde reactions, which leads to lower *P-T* results estimated from the unresorbed rim composition of garnets than the true conditions. Through qualitative reconstruction of the compositions of clinopyroxene, original modal proportions and rim composition of garnet, this study yielded peak metamorphic conditions of ~15–17 kbar/~790–810 °C. These results are similar to those for other Paleoproterozoic high-pressure granulites and moderate-temperature eclogites worldwide (Brown and Johnson, 2018, and references therein). The metamorphic conditions contrast with those of Archean metamorphic terranes, which are predominantly characterized by high-temperature and low- to moderate-pressure metamorphic conditions (e.g., Windley, 1995; Brown, 2007; Brown and Johnson, 2018; Holder et al., 2019; Palin et al., 2020). The high *P-T* regimes, clockwise *P-T* histories, and rapid tectonic exhumation histories of the Paleoproterozoic high-pressure granulite and eclogite terranes suggest that the tectonic processes could probably be compared with those

under modern plate tectonics, although these rocks document relatively higher apparent thermal gradients (~14–16 °C/km). A statistical evaluation of *T*/*P* over time demonstrates that bimodal metamorphism has become a global scale since the early Paleoproterozoic (~2.2 Ga) to tthe present day (Holder et al., 2019), and the higher thermal gradients might be explained by the gradual development of modern plate tectonic regimes with secular cooling of the mantle (Holder et al., 2019; Brown and Johnson, 2018; Palin et al., 2020). Together with recently recognized ~1.80 Ga eclogite xenoliths from magmatic carbonate in the adjacent area (Xu et al., 2018), it seems to infer that mordern-style tectonics might have operated as far back as the Paleoproterozoic (~1.95–1.80 Ga) from the NCC (Xu et al., 2018; Zhai et al., 1995; Zhao et al., 2001; Zhou et al., 2017).

7. Conclusions

1. The garnet grains of the investigated mafic granulites preserve conspicuous microstructural and chemical zoning patterns. Microstructurally, they show a zonal distribution of frozen mineral inclusions. The first is a poikilitic core including considerable amount of quartz, with minor plagioclase, titanite, ilmenite, clinopyroxene and apatite. The second is a rutile-bearing, inclusion-poor mantle. The third is a resorbed rim characterized by breakdown textures. Chemically, garnets exhibit pronounced zoning, with bell-shaped X_{Sps}, initially flat and then increasing/decreasing X_{Pyr} and Fe#, and initially increasing and then decreasing X_{Grs} from cores to mantles, and resorbed rims. Both zoning patterns suggest that granulitic garnets in the studied sample record a complete history of early progressive to late retrogressive metamorphism.
2. Metamorphic history can be divided into early prograde (M_{1-1}), late prograde (M_{1-2}), near peak (M_{2-1}), peak (M_{2-2}), isothermal decompression (M_3), and isobaric cooling (M_4) stages. M_{1-1} features the garnet poikilitic core and its inclusions, with maximum X_{Sps} and Fe# and minimum X_{Pyr}. M_{1-2} is characterized by inclusion-type minerals in the garnet core-mantle boundary, accompanied by maximum X_{Grs} and inflection points for X_{Pyr} and Fe#. M_{2-1} features the occurrence of rutile in garnet mantles and other minerals in the matrix, with a presently preserved maximum X_{Pyr} and minimum Fe#. M_{2-2} should have been recorded in the garnet rim, although the domain broke down into other minerals and the original information was lost. M_3 is characterized by the breakdown of garnet into plagioclase and pyroxene, and clinopyroxene porphyroblasts into plagioclase blebs and diopsidic clinopyroxene, with rare orthopyroxene and hornblende. M_4 is characterized by retrogression of amphibolite-facies. These generation assemblages together define a clockwise *P*-*T* path.
3. The conditions are estimated at 6–9 kbar/600–700 °C (M_{1-1}), 9–11.2 kbar/680–740 °C (M_{1-2}), 12–15 kbar/735–785 °C (M_{2-1}), >13.5 kbar/>760 °C (M_{2-2}), 7–10 kbar/~800–850 °C (M_3) and 3–5 kbar/ 650–680 °C (M_4), respectively. Although the peak metamorphic stage (M_{2-2}) information is modified by retrograde reactions, the conditions are further constrained to ~15–17 kbar/ ~790–810 °C through qualitative reconstruction of the composition of clinopyroxene, original modal proportions and rim composition of garnet.
4. The preservation of growth zoning in garnet and the near-isothermal decompression path suggests that the host rocks probably experienced a short-lived peak metamorphic stage and a rapid tectonic exhumation process.
5. Metamorphic records of the mafic granulites from the northern Hengshan area were probably a response to subduction-collision-exhumation processes involved in the assembly of the NCC during the Paleoproterozoic. This suggests that the Paleoproterozoic (~1.95–1.80 Ga) tectonic processes are similar to those under the modern plate tectonic regimes, although their relatively higher apparent thermal gradients (14–16 °C/km).

Declaration of Competing Interest

The authors declare that they have no known competing financial interests or personal relationships that could have appeared to influence the work reported in this paper.

Acknowledgements

This manuscript was written and modified according to a conference report titled 'Garnet perspectives into metamorphic evolution of granulites: Cases study from the North China Craton' by the first author, 2018 International Symposium on Granulite Facies Metamorphism and Early Plate Tectonics, held in 23-28 Oct Laiyang, Shandong Province, China. The Co-Editor-in-Chief Prof. Greg Shellnutt and the Managing Guest editor Prof. Chang Whan Oh of this special issue are thanked.. Prof. Tatsuki Tsujimori, and two anonymous reviewers are thanked for their constructive suggestions, critical but helpful comments, which have led to great improvements in the quality of this article. Prof. Jinghui Guo, Liang Liu, Chunjing Wei and Dr. Yi Zou are appreciated for their helpful discussions and comments. Dr. Wenqiang Yang is thanked for his enthusiastic help during EPMA analysis. This study was financially supported by the research programs (Grant No. 41890834, 41702196, 41703023) of the Natural Science Foundation of China, the Opening Foundation of State Key Laboratory of Continental Dynamics, Northwest University (18LCD12), the basic research programs (2020JQ-355, 2019JM-056) of the Shaanxi Provincial Department of Science and Technology, and the Fundamental Research Funds for the Central Universities, CHD, China (300102279302).

References

Baldwin, J.A., Powell, R., Williams, M.L., Goncalves, P., 2007. Formation of eclogite, and reaction during exhumation to mid-crustal levels, snowbird tectonic zone, western canadian shield. J. Metamorph. Geol. 25, 953–974.
Bhadra, S., Bhattacharya, A., 2007. The barometer tremolite- tschermakite + 2 albite = 2 pargasite + 8 quartz: constraints from experimental data at unit silica activity, with application to garnet-free natural assemblages. Am. Mineral. 92, 491–502.
Bhattacharya, A., Krishnakumar, K.R., Raith, M., Sen, S.K., 1991. An improved set of a-X parameters for Fe-Mg-Ca garnets and refinements of the orthopyroxene-garnet thermometer and the orthopyroxene-garnet-plagioclase-quartz barometer. J. Petrol. 32, 629–656.
Brown, M., 2007. Metamorphic conditions in orogenic belts: a record of secular change. Int. Geol. Rev. 49, 193–234.
Brown, M., Johnson, T., 2018. Secular change in metamorphism and the onset of global plate tectonics. Am. Mineral. 103 (2), 181–196.
Brown, D.A., Tamblyn, R., Hand, M., Morrissey, L.J., 2020. Thermobarometric constraints on burial and exhumation of 2-billion-yearold eclogites and their metapelitic hosts. Precambrian Res. 347, 105833.
Caddick, M.J., Kohn, M.J., 2013. Garnet: Witness to the evolution of destructive plate boundaries. Elements 9, 427–432.
Caddick, M.J., Konopasek, J., Thompson, A.B., 2010. Preservation of garnet growth zoning and the duration of prograde metamorphism. J. Petrol. 51 (11), 2327–2347.
Carlson, W.D., 2002. Scales of disequilibrium and rates of equilibration during metamorphism. Am. Mineral. 87 (2–3), 185–204.
Cheng, H., Cao, D.D., 2013. Recent advances in garnet Lu-Hf geochronology and its applications inthe Dabie orogen. Chin. Sci. Bull. 58, 2271–2278.
Chu, X., Ague, J.J., Meng, T., Baxter, E.F., Douglas, R., Page, C.C., 2018. Testing for rapid thermal pulses in the crust by modeling garnet growth-diffusion-resorption profiles in a UHT metamorphic "hot spot", New Hampshire, USA. J. Petrol. 59, 1939–1964.
Cooke, R.A., O'Brien, P.J., Carswell, D.A., 2000. Garnet zoning and the identification of equilibrium mineral compositions in high-pressure-temperature granulites from the Moldanubian zone, Austria. J. Metamorph. Geol. 18, 551–569.
Droop, G.T.R., 1987. A general equation for estimating Fe^{3+} concentrations in ferromagnesian silicates and oxides from microprobe analyses, using stoichiometric criteria. Mineral. Mag. 51, 431–435.
Eckert Jr., J.O., Newton, R.C., Kleppa, O.J., 1991. The ΔH of reaction and recalibration of garnet - pyroxene - plagioclase - quartz geobarometers in the CMAS system by solution calorimetry. Am. Mineral. 76, 148–160.
Gaidies, F., Capitani, C.D., Abart, R., 2008. THERIA_G: a software program to numerically model prograde garnet growth. Contrib. Mineral. Petrol. 155 (5), 657–671.
Gaidies, F., Morneau, Y.E., Petts, D.C., Jackson, S.E., Zagorevski, A., Ryan, J.J., 2020. Major and trace element mapping of garnet: Unravelling the conditions, timing and rates of metamorphism of the Snowcap assemblage, west-central Yukon. J. Metamorph. Geol. 00, 1–32.
Green, E.C.R., White, R.W., Diener, J.F.A., Powell, R., Holland, T.J.B., Palin, R.M., 2016. Activity-composition relations for the calculation of partial melting equilibria in metabasic rocks. J. Metamorph. Geol. 34, 845–869.

Guo, J.H., O'Brien, P.J., Zhai, M.G., 2002. High-pressure granulites in the Sanggan area, North China Craton: metamorphic evolution, P-T paths and geotectonic significance. J. Metamorph. Geol. 20, 741–756.
Halls, H.C., Li, J.H., Davis, D., Hou, G.T., Zhang, B.X., Qian, X.L., 2000. A precisely dated Proterozoic palaeomagnetic pole from the North China Craton, and its relevance to palaeocontinental reconstruction. Geophys. J. Int. 143, 185–203.
Harley, S.L., 1989. The origins of granulites: a metamorphic perspective. Geol. Mag. 126, 215–247.
Higashino, F., Rubatto, D., Kawakami, T., Bouvier, A.S., Baumgartner, L.P., 2019. Oxygen isotope speedometry in granulite facies garnet recording fluid/melt–rock interaction (Sør Rondane Mountains, East Antarctica). J. Metamorph. Geol. 37, 1037–1048.
Holder, R.M., Viete, D.R., Brown, M., Johnson, T.E., 2019. Metamorphism and the evolution of plate tectonics. Nature 572 (7769), 378–381.
Holland, T.J.B., Blundy, J.D., 1994. Non-ideal interactions in calcic amphiboles and their bearing on amphibole-plagioclase thermometry. Contrib. Mineral. Petrol. 116, 433–447.
Holland, T.J.B., Powell, R., 1998. An internally consistent thermodynamic data set for phases of petrological interest. J. Metamorph. Geol. 16, 309–343.
Holland, T.J.B., Powell, R., 2003. Activity-composition relations for phases in petrological calculations: an asymmetric multicomponent formulation. Contrib. Mineral. Petrol. 145, 492–501.
Holland, T.J.B., Powell, R., 2011. An improved and extended internally consistent thermodynamic dataset for phases of petrological interest, involving a new equation of state for solids. J. Metamorph. Geol. 29 (3), 333–383.
Hollis, J.A., Harley, S.L., White, R.W., Clarke, G.L., 2006. Preservation of evidence for prograde metamorphism in ultrahigh-temperature, high-pressure kyanite-bearing granulites, south harris, scotland. J. Metamorph. Geol. 24 (3), 263–279.
Kröner, A., Wilde, S.A., O'Brien, P.J., Li, J.H., Passchier, C.W., Walte, N.P., Liu, D.Y., 2005. Field relationships, geochemistry, zircon ages and evolution of a late Archean to Paleoproterozoic lower crustal section in the Hengshan Terrain of Northern China. Acta Geol. Sin. 79, 605–629 (English Edition.).
Kröner, A., Wilde, S.A., Zhao, G.C., O'Brien, P.J., Sun, M., Liu, D.Y., Wan, Y.S., Liu, S.W., Guo, J. H., 2006. Zircon geochronology of mafic dykes in the Hengshan Complex of northern China: evidence for late Palaeoproterozoic rifting and subsequent high-pressure event in the North China Craton. Precambrian Res. 146, 45–67.
Lal, R.K., 1993. Internally consistent recalibrations of mineral equilibria for geothermobarometry involving garnet–orthopyroxene–plagioclase–quartz assemblages and their application to the South Indian granulites. J. Metamorph. Geol. 11, 855–866.
Li, J.H., Qian, X.L., 1994. The early Precambrian crustal evolution of Hengshan metamorphic terrane, North China Craton. Shanxi Science and Technology Press, Taiyuan p. 1-36. in Chinese with English abstract.
Li, J.H., Zhai, M.G., Qian, X.L., Guo, J.H., Wang, Y.G., Yan, Y.H., Li, Y.G., 1998. The geological occurrence, regional tetonic setting and exhumation of late Archean high-pressure granulite within the high-grade metamorphic terranes, north to central portion of North China Craton. Acta Petrol. Sin. 14 (2), 176–189.
Liu, F., Zhang, L., Li, X., Slabunov, A.I., Wei, C., Bader, T., 2017. The metamorphic evolution of paleoproterozoic eclogites in kuru-vaara, northern Belomorian Province, Russia: Constraints from P-T pseudosections and zircon dating. Precambrian Res. 289, 31–47.
Loose, D., Schenk, V., 2018. 2.09 Ga old eclogites in the Eburnian-Transamazonian orogen of southern Cameroon: significance for Palaeoproterozoic plate tectonics. Precambrian Res. 304, 1–11.
Maruyama, S., Masago, D., Katayama, I., Iwase, Y., Toriumi, M., Omori, S., Aoki, K., 2010. A new perspective on metamorphism and metamorphic belts. Gondwana Res. 18 (1), 106–137.
Möller, C., 1998. Decompressed eclogites in the Sveconorwegian (−Grenvillian) orogen of SW Sweden Petrology and tectonic implications. J. Metamorph. Geol. 16, 641–656.
Müller, S., Dziggel, A., Kolb, J., Sindern, S., 2018. Mineral textural evolution and PTpath of relict eclogite-facies rocks in the paleoproterozoic Nagssugtoqidian Orogen, South-East Greenland. Lithos 296, 212–232.
Newton, R.C., Perkins, D., 1982. Thermodynamic calibration of geobarometers based on the assemblages garnet - orthopyroxene,clinopyroxene - plagioclase - quartz. Am. Mineral. 67, 203–222.
O'Brien, P.J., Walte, N., Li, J., 2005. The petrology of two distinct granulite types in the Hengshan Mts, China, and tectonic implications. J. Asian Earth Sci. 24 (5), 615–627.
Palin, R.M., Santosh, M., Cao, W., Li, S., Hernandez-Uribe, D., Parsons, A.J., 2020. Secular change and the onset of plate tectonics on Earth. Earth-Science Reviews 207, 103172.
Parkinson, C.D., 2000. Coesite inclusions and prograde compositional zonation of garnet in whiteschist of the HP-UHPM Kokchetav massif, Kazakhstan: a record of progressive UHP metamorphism. Lithos 52, 215–233.
Peng, P., Zhai, M., Zhang, H., Guo, J., 2005. Geochronological constraints on early Proterozoic evolution of the North China Block: SHRIMP zircon ages of different types of dykes. Int. Geol. Rev. 47, 492–508.
Perchuk, A.L., Morgunova, A.A., 2014. Variable P–T paths and HP-UHP metamorphism in a Precambrian terrane, Gridino, Russia: petrological evidence and geodynamic implications. Gondwana Res. 25, 614–629.
Powell, R., 1985. Regression diagnostic and robust regression in geothermometer / geobarometer calibration: the garnet - clinopyroxene geothermometer revisited. J. Metamorph. Geol. 3, 231–243.
Powell, R., Holland, T.J.B., 1988. An internally consistent dataset with uncertainties and correlations 3: applications to geobarometry, worked examples and a computer program. J. Metamorph. Geol. 6, 173–204.
Qian, J.H., Wei, C.J., 2016. P–T–t evolution of garnet amphibolites in theWutai–Hengshan area, North China Craton: insights from phase equilibria and geochronology. J. Metamorph. Geol. 34, 423–446.
Qian, J., Yin, C., Wei, C., Zhang, J., 2019. Two phases of Paleoproterozoicmetamorphismin the Zhujiafang ductile shear zone of the Hengshan complex: Insights into the tectonic evolution of the North China Craton. Lithos 330-331, 35–54.
Ravna, E.K., 2000. The garnet-clionopyroxene Fe^{2+}-Mg geothermometer: an updated calibration. J. Metamorph. Geol. 18, 211–219.
Ringwood, A.E., 1975. Composition and Petrology of the Earth's Mantle. McGraw-Hill, London, New York and Sydney 618 p.
Rubatto, D., Burger, M., Lanari, P., Hattendorf, B., Schwarz, G., Neff, C., Schmidt, P.K., Hermann, J., Vho, A., Gunther, D., 2020. Identification of growth mechanisms in metamorphic garnet by high-resolution trace element mapping with LA-ICP-TOFMS. Contrib. Mineral. Petrol. 175, 61.
Sizova, E., Gerya, T., Brown, M., Perchuk, L.L., 2010. Subduction styles in the Precambrian: insight from numerical experiments. Lithos 116, 209–229.
Spear, F.S., 1993. Metamorphic Phase Equilibria and Pressure-Temperature-Time Paths. Mineralogical Society of America, Chantilly, VA Monograph 1,799 pp.
Spear, F.S., 2014. The duration of near-peak metamorphism from diffusion modelling of garnet zoning. J. Metamorph. Geol. 32, 903–914.
Tomkins, H.S., Powell, R., Ellis, D.J., 2007. The pressure dependence of the zirconium-in-rutile thermometer. J. Metamorph. Geol. 25 (6), 703–713.
Trap, P., Faure, M., Lin, W., Augier, R., Fouassier, A., 2011. Syn-collisional channel flow and exhumation of Paleoproterozoic high-pressure rocks in the Trans-North China Orogen: the critical role of partial-melting and orogenic bending. Gondwana Res. 20, 498–515.
Trap, P., Faure, M., Lin, W., Breton, N.L., Monié, P., 2012. Paleoproterozoic tectonic evolution of the Trans-North China Orogen: toward a comprehensive model. Precambrian Res. 222, 191–211.
Wan, B., Windley, B.F., Xiao, W., Feng, J., Zhang, J., 2015. Paleoproterozoic high-pressure metamorphism in the northern North China Craton and implications for the Nuna supercontinent. Nat. Commun. 6, 8344.
Wang, R.M., Chen, Z.Z., Chen, F., 1991. Grey tonalitic gneiss and high-pressure granulite inclusions in Hengshan, Shanxi Province, and their geological significance. Acta Petrol. Sin. 4, 36–45 (in Chinese with English abstract).
Wei, C.J., 2018. Paleoproterozoic metamorphism and tectonic evolution in Wutai-Hengshan region, Trans-North China Orogen. Earth Sci. 43 (1), 24–43 (in Chinese with English abstract).
Wei, C.J., Qian, J.H., Zhou, X.W., 2014. Paleoproterozoic crustal evolution of the Hengshan-Wutai-Fuping region, North China Craton. Geosci. Front. 54, 85–497.
Weller, O.M., StOnge, M.R., 2017. Record of modern-style plate tectonics in the Palaeoproterozoic Trans-Hudson Orogen. Nat. Geosci. 10 (4), 305–311.
White, R.W., Powell, R., Holland, T.J.B., 2007. Progress relating to calculation of partial melting equilibria for metapelites. J. Metamorph. Geol. 25, 511–527.
White, R.W., Powell, R., Holland, T., Johnson, T.E., Green, E.C.R., 2014. New mineral activity-composition relations for thermodynamic calculations in metapelitic systems. J. Metamorph. Geol. 32, 261–286.
Whitney, D.L., Evans, B.W., 2010. Abbreviations for names of rock-forming minerals. Am. Mineral. 95, 185–187.
Windley, B.F., 1995. The Evolving Continents. 3th Ed. Chichester, England, John Wiley Sons.
Wu, J.L., Zhang, H.F., Zhai, M.G., Guo, J.H., Liu, L., Yang, W.Q., Wang, H.Z., Zhao, L., Jia, X.L., Wang, W., 2016. Discovery of pelitic high-pressure granulite from Manjinggou of the Huai'an complex, North China Craton: Metamorphic P-T evolution and geological implications. Precambrian Res. 278, 323–336.
Wu, J., Zhang, H., Zhai, M., Guo, J., Li, R., Wang, H., Zhao, L., Jia, X., Wang, L., Hu, B., Zhang, H., 2017. Paleoproterozoic high-pressure-high-temperature pelitic granulites from Datong in the North China Craton and their geological implications: Constraints from petrology and phase equilibrium modeling. Precambrian Res. 303, 727–748.
Wu, J., Zhai, M., Zhang, H., Guo, J., Wang, H., Yang, W., Zhang, H., Hu, B., 2018a. Petrologic indicators of prograde metamorphism in Paleoproterozoic garnet mafic granulites from the Huai'an complex. North China Craton: Science Bulletin 63, 81–84.
Wu, J.L., Zhai, M.G., Zhang, H.F., Hu, B., 2018b. An analysis of mineralogical characteristics and metamorphism of Paleoproterozoic pelitic granulites from Datong-Huai'an area, the North China Craton. Acta Petrol. Sin. 34 (11), 3266–3286 (in Chinese with English abstract).
Wu, J., Zhang, H., Zhai, M., Zhang, H., Wang, H., Li, R., Hu, B., Zhang, H., 2019. Shared metamorphic histories of various Palaeoproterozoic granulites from Datong-Huai'an area, North China Craton,NCC: Constraints from zircon U-Pb ages and petrology. Int. Geol. Rev. 61 (6), 694–719.
Xu, C., Kynicky, J., Song, W.L., Tao, R.B., Lu, Z., Li, Y.X., Yang, Y.C., Pohanka, M., Galiova, M.V., Zhang, L.F., Fei, Y.W., 2018. Cold deep subduction recorded by remnants of a Paleoproterozoic carbonated slab. Nat. Commun. 9.
Zhai, M.G., 2009. Two kinds of granulites,HT-HP and HT-UHT in North China Craton:their genetic relation and geotectonic implications. Acta Petrol. Sin. 25, 1753–1771 (in Chinese with English abstract).
Zhai, M.G., 2012. Evolution of the North China Craton and early plate tectonics. Acta Geol. Sin. 86 (9), 1335–1349 (in Chinese with English abstract).
Zhai, M.G., Liu, W.J., 2003. Palaeoproterozoic tectonic history of the North China Craton: a review. Precambrian Res. 122, 183–199.
Zhai, M.G., Guo, J.H., Yan, Y.H., Li, Y.G., Han, X.L., 1992. The discovery of high-pressure basic granulite in the Archaean north China Craton and preliminary study. Sci. China 12, 1325–1330 (in Chinese).
Zhai, M.G., Guo, J.H., Li, J.H., Yan, Y.H., Li, Y.G., Zhang, W.H., 1995. The discoveries of retrograde eclogites in North China craton in Archaean. Chin. Sci. Bull. 40, 1590–1594.
Zhang, J., Zhao, G.C., Li, S.Z., Sun, M., Liu, S.W., Wilde, S.A., Kröner, A., Yin, C.Q., 2007. Structural geology of the Hengshan-Wutai-Fuping mountain belt: Implications for the tectonic evolution of the Trans-North China Orogen. J. Struct. Geol. 29 (6), 933–949.

Zhang, H.F., Wang, H.Z., Santosh, M., Zhai, M.G., 2016a. Zircon U-Pb ages of Paleoproterozoic mafic granulites from the Huai'an terrane, North China Craton (NCC): Implications for timing of cratonization. Precambrian Res. 272, 244–263.

Zhang, D.D., Guo, J.H., Tian, Z.H., Liu, F., 2016b. Metamorphism and P-T evolution of high pressure granulite in Chicheng, northern part of the Paleoproterozoic Trans-North China Orogen. Precambrian Res. 280, 76–94.

Zhang, Y.H., Wei, C.J., Lu, M.J., Zhou, X.W., 2018. P-T-t evolution of the high-pressure mafic granulites from northern Hengshan, North China Craton: insights from phase equilibria and geochronology. Precambrian Res. 312, 1–15.

Zhang, Y.Y., Wei, C.J., Chu, H., 2020a. Paleoproterozoic oceanic subduction in the North China Craton: insights from the metamorphic P–T–t paths of the Chicheng Mélange in the Hongqiyingzi complex. Precambrian Res. 342, 105671.

Zhang, L., Wu, J.L., Tu, J.R., Wu, D., Li, N., Xia, X.P., Ren, Z.Y., 2020b. RMJG rutile: a new natural reference material for microbeam U-Pb dating and Hf isotopic analysis geostandards and geoanalytical research. 44 (1), 133–145.

Zhao, G.C., Cawood, P.A., Wilde, S.A., Lu, L.Z., 2001. High-pressure granulites,retrograded eclogites from the Hengshan Complex, North China Craton: petrology and tectonic implications. J. Petrol. 42, 1142–1170.

Zhao, G.C., Sun, M., Wilde, S.A., Li, S.Z., 2005. Late Archean to Paleoproterozoic evolution of the North China Craton: key issues revisited. Precambrian Res. 136, 177–202.

Zhao, R.F., Guo, J.H., Peng, P., Liu, F., 2011. 2.1 Ga crustal remelting event in Hengshan complex: evidence from zircon U-Pb dating and Hf-Nd isotope study on potassic granites. Acta Petrol. Sin. 27 (6), 1607–1623.

Zhou, L.G., Zhai, M.G., Lu, J.S., Zhao, L., Wang, H.Z., Wu, J.L., Liu, B., Shan, H.X., Cui, X.H., 2017. Paleoproterozoic metamorphism of high-grade granulite facies rocks in the North China Craton: study advances, questions and new issues. Precamb. Res. 303, 520–547.

Zou, Y., Chu, X., Li, Q.L., Mitchell, R.N., Zhai, M.G., Zhu, X.Y., Zhao, L., Wang, Y.Q., Liu, B., 2020. Local rapid exhumation and fast cooling in a long-lived paleoproterozoic orogeny. J. Petrol. 61 (10) egaa091.